Meex RC, Hoy AJ, Morris A, Brown RD, Lo JC, Burke M, Goode RJ, Kingwell BA, Kraakman MJ, Febbraio MA, Greve JW, Rensen SS, Molloy MP, Lancaster GI, Bruce CR, Watt MJ. Fetuin B is a secreted hepatocyte factor linking steatosis to impaired glucose metabolism. Cell Metab 2015;22(6):1078-89.

http://hdl.handle.net/11187/2369

Fetuin B is a secreted hepatocyte factor linking steatosis to impaired glucose metabolism

Ruth C. Meex[1], Andrew J. Hoy[1], Alexander Morris[1], Russell D. Brown[1], Jennifer C.Y. Lo[1], Melissa Burke[2,3], Robert J.A. Goode[4], Bronwyn A. Kingwell[5], Michael J. Kraakman[5], Mark A. Febbraio[5,6], Jan Willem Greve[7], Sander S. Rensen[7], Mark P. Molloy[8], Graeme I. Lancaster[5], Clinton R. Bruce[1], Matthew J. Watt[1]

[1] Monash Biomedicine Discovery Institute, Metabolic Disease and Obesity Program, and Biology of Lipid Metabolism laboratory, Department of Physiology, Monash University, Clayton, Victoria, 3800, Australia.

[2] Biotechnology Research Laboratories, Department of Physiology, Monash University, Clayton, Victoria, 3800, Australia.

[3] The Francis Crick Institute, Mill Hill Laboratory, London, United Kingdom, NW7 1AA.

[4] Department of Biochemistry and Molecular Biology, Monash University, Clayton, Victoria, 3800, Australia.

[5] Baker IDI Heart and Diabetes Institute, Melbourne, Victoria, 3004, Australia.

[6] The Garvan Institute of Medical Research, Sydney, NSW, 2010, Australia

[7] NUTRIM School of Nutrition and Translational Research in Metabolism, Maastricht University Medical Centre, Department of General Surgery, Maastricht, The Netherlands.

[8] Australian Proteome Analysis Facility, Macquarie University, Sydney, NSW, 2109, Australia.

Contact Information

Matthew J. Watt, Ph.D.

Department of Physiology, Monash University, Clayton, Victoria, 3800, Australia

Phone: 613 9905 2584. Fax: 613 9905 2547.

Email: matthew.watt@monash.edu

Footnotes

Current address for CRB is Centre for Physical Activity and Nutrition Research, School of Exercise and Nutrition Science, Deakin University, Burwood, Victoria, 3125, Australia.

Current address for AJH is Discipline of Physiology, School of Medical Sciences and Bosch Institute, University of Sydney, NSW, 2006, Australia

Summary

Liver steatosis is associated with the development of insulin resistance and the pathogenesis of type 2 diabetes. We tested the hypothesis that protein signals originating from steatotic hepatocytes communicate with other cells to modulate metabolic phenotypes. We show that the secreted factors from steatotic hepatocytes induce pro-inflammatory signaling and insulin resistance in cultured cells. Next, we identified 168 hepatokines, of which 32 were differentially secreted in steatotic versus non-steatotic hepatocytes. Targeted analysis showed that fetuin B was increased in humans with liver steatosis and patients with type 2 diabetes. Fetuin B impaired insulin action in myotubes and hepatocytes and caused glucose intolerance in mice. Silencing of fetuin B in obese mice improved glucose tolerance. We conclude that the protein secretory profile of hepatocytes is altered with steatosis and is linked to inflammation and insulin resistance. Thus, preventing steatosis may limit the development of dysregulated glucose metabolism in settings of overnutrition.

Introduction

The liver plays a central role in systemic glucose and lipid metabolism. Accumulation of excess lipid in the liver, clinically known as hepatic steatosis, is an abnormality that characterises obesity and type 2 diabetes. Steatosis develops largely as a consequence of caloric overload and is rapidly reversed upon consumption of a hypocaloric diet (Petersen et al., 2005). Steatosis is a component of non-alcoholic fatty liver disease (NAFLD) (Day and James, 1998), which is a serious medical condition affecting ~20-40% of adults in the United States (Browning et al., 2004) and ~70% of morbidly obese individuals (Bellentani et al., 2000). NAFLD precedes the development of non-alcoholic steatohepatitis (NASH) and is closely linked with other metabolic disorders including insulin resistance, type 2 diabetes, dyslipidemia and cardiovascular disease (Chitturi et al., 2004). The factors linking these disorders remain unresolved.

Hepatic lipid content is regulated by a complex interplay between free fatty acid uptake and oxidation, uptake of fatty acids from chylomicron-derived triglycerides, triglyceride synthesis through fatty acid re-esterification and *de novo* lipogenesis, and triglyceride secretion contained within very-low density lipoproteins (Samuel and Shulman, 2012). Hence, defects within any of these processes can cause an imbalance between lipid supply and demand, and subsequently drive hepatic steatosis. Hepatic steatosis in rodents develops rapidly in the setting of over-nutrition (Kraegen et al., 1991; Stewart et al., 2009; Turner et al., 2013), and occurs at a time point that normally precedes the development of other abnormalities associated with caloric excess including adipocyte hypertrophy and obesity development (Strissel et al., 2007), adipocyte death (Strissel et al., 2007), macrophage infiltration and inflammation of adipose tissue (Strissel et al., 2007; Turner et al., 2013; Xu et al., 2003), skeletal muscle lipid accumulation, insulin resistance (Kraegen et al., 1991; Turner et al., 2013), whole-body hyperglycemia and hyperinsulinemia (Turner et al., 2013; Xu et al.,

2003). Targeted studies have identified several liver-derived endocrine factors that impact peripheral metabolism including fetuin A (Pal et al., 2012), adropin (Kumar et al., 2008), angiopoietin-like protein 6 (Angptl6) (Oike et al., 2005), fibroblast growth factor 21 (FGF21) (Kharitonenkov et al., 2005) and selenoprotein P (Misu et al., 2010), demonstrating that factors secreted from hepatocytes, or hepatokines, are involved in metabolic cross-talk. Furthermore, cDNA microarray and proteomic studies have reported changes in intracellular gene expression and protein content of whole liver with caloric overload in rodents and humans (Kirpich et al., 2010; Toye et al., 2007; Younossi et al., 2005; Zhang et al., 2010). Collectively, these observations are consistent with the notion that liver steatosis is an early manifestation in the aetiology of metabolic dysfunction associated with caloric (fatty acid) overload, and that protein signals originating from the steatotic liver may 'cross-talk' with other tissues to influence metabolic and inflammatory function, and thereby modulate metabolic phenotypes.

The aim of this study was to test whether hepatic steatosis, independent of inflammation, alters the hepatocyte protein secretory profile, and to test whether changes in the secretory products contribute to the development of metabolic dysfunction in other cell types. We show that liver steatosis alters the hepatokine secretion profile and produces a milieu that induces inflammation and insulin resistance in macrophages and skeletal muscle. Using discovery-based 'omics' platforms, we identify fetuin-B as a liver-secreted protein that is elevated in patients with liver steatosis and type 2 diabetes, and causes glucose intolerance in mice.

Results

Short-term high fat feeding of C57Bl6/J mice causes hepatic steatosis and glucose intolerance, but not inflammation or liver damage

The liver is composed of many cell types including hepatocytes, stellate cells, endothelial cells and numerous immune cell types. To identify hepatocyte-specific factors that are induced by steatosis, we developed an *ex vivo* model in which hepatocytes were isolated from mice that had been fed either a standard chow or high fat diet (HFD) for 6 weeks. At the time of hepatocyte isolation, the mice fed a HFD exhibited increased body mass, increased epididymal fat mass and glucose intolerance compared with chow-fed mice (Fig. S1A-C). Plasma ALT and AST levels were unaffected by high-fat feeding, demonstrating that the diet did not cause liver damage (Fig. S1D).

Isolated hepatocytes from high fat fed mice are steatotic in the absence of inflammation

The purity of the hepatocyte isolation was first confirmed by flow cytometry and immunofluorescent staining. Incubation of the isolated cells with a FITC-conjugated anti-albumin antibody resulted in a shift in fluorescence intensity of the entire cell population (Fig. 1A), demonstrating a highly pure hepatocyte population. There was no evidence of endothelial cells ($CD31^+$) in the isolated cell population, and macrophages/Kupffer cells ($CD45^+$ $F4/80^+$ cells) made up just 2.3% of the cell population (Fig. 1B). Hepatocytes isolated from HFD mice were fat-laden, as demonstrated by large and abundant intracellular lipid droplets (Fig. 1C) and increased intracellular triacylglycerol content (Fig. 1D). Steatosis can be accompanied by inflammation *in vivo*; however, there was no indication of proinflammatory serine/threonine kinase activation as demonstrated by analysis of c-Jun terminal kinase (JNK) phosphorylation (indicating activity) and by a lack of IκBα degradation (indicating activation of NFκB signalling) (Fig. 1E). These data establish a model in which hepatocytes are steatotic, but are neither inflamed nor damaged, as occurs in

NASH, and allow us to next determine the effect of simple steatosis on the hepatocyte secretome.

Secreted products from steatotic hepatocytes regulate inflammation and insulin action in other cell types: evidence of metabolic cross-talk

The induction of liver steatosis is associated with obesity-related disorders such as insulin resistance, inflammation and dysregulated lipid metabolism (Abdul-Ghani et al., 2008; Kraegen et al., 1991; Larson-Meyer et al., 2011; Wicklow et al., 2012). In an attempt to model this pathophysiology *in vitro*, cultured myotubes and macrophages were incubated for 24 h in the conditioned medium (CM) produced by hepatocytes from Chow and HFD fed mice. Cells were then washed prior to functional assays to evaluate the metabolic and inflammatory responses of cells to the hepatocyte secreted products.

Skeletal muscle is a major site for fatty acid metabolism and insulin-stimulated glucose disposal. Glucose uptake in L6 GLUT4myc myotubes was not different between Chow and HFD CM in the basal (unstimulated) state. Insulin increased glucose uptake by 110% in myotubes exposed to Chow CM and by only 53% in myotubes exposed to HFD CM (Fig. 1F), demonstrating impaired insulin action. Short-term (2 h) exposure to the HFD CM did not impair insulin action (data not shown), suggesting that the HFD-CM was not directly impairing insulin signalling, but was instead affecting other processes that impact insulin action. We reasoned that the decline in insulin action was associated with alterations in fatty acid metabolism, given the close association between these processes (Turner et al., 2013). Indeed, myotubes incubated in HFD CM showed a small, but significant, increase in fatty acid uptake (12%), oxidation (10%) and triglyceride storage rates (14%) (Fig. 1G); although we did not observe changes in diglyceride storage rates (Fig. 1G).

Low-grade inflammation is often associated with HFD-induced insulin resistance. Incubation of macrophages with Chow CM did not affect inflammatory signalling when compared with untreated cells (data not shown). The HFD CM induced a pro-inflammatory response as demonstrated by increased phosphorylation of JNK and IKK (Fig. 1H). Interestingly, pre-incubation of macrophages in HFD CM also exacerbated the lipopolysaccharide (LPS)-induced inflammation (Fig. 1H). Together, these experiments indicate that steatotic hepatocytes secrete products that induce selective components of pro-inflammatory pathways in macrophages and cause insulin resistance in skeletal muscle.

Steatosis regulates the protein secretome in hepatocytes

Having determined that steatotic hepatocytes secrete factors that influence the function of other cells, we next attempted to identify hepatocyte-derived secretory proteins involved in steatosis-induced metabolic dysregulation. A major challenge in assessing the hepatocyte secretome is delineating the contribution of hepatocytes from other cell types that reside in the liver. To overcome this limitation, we utilised the cell-based model of purified hepatocytes described above (Fig. 1A-B). A second challenge associated with this model is determining the contribution of cytosolic contamination to the secretory profile. Cell death (trypan blue staining) was not different between hepatocytes exposed to collection medium for 0 or 24 h, or between hepatocytes derived from Chow or HFD fed mice (Fig. S2A). In support of this finding, lactate dehydrogenase levels in the culture medium were not different between Chow and HFD hepatocytes (Fig. S2C). The major non-muscle cytoskeletal actin, β-actin, was not detected in the cell culture medium by immunoblot (0, 8 and 24 h; Fig. S2B), and 39 of the 50 most abundant proteins detected in the culture medium are known secreted proteins (Table S1). Thus, while cell death is inevitable, this was negligible, and the release of intracellular proteins into the 'collection medium' was not different between treatment groups.

We cross-referenced the sequence of proteins detected in the conditioned medium with algorithms to predict classically secreted proteins that harbour an N-terminal signal sequence. Proteins that were detected in the culture medium without an N-terminal signal sequence could be secreted by non-classical secretion mechanisms; however, for the purpose of these experiments they were treated as 'non-secreted' unless expressly annotated as secreted in UniProt.

iTRAQ-based proteomic analysis identified and quantitated 538 proteins; 370 which were designated 'non-secreted' and 168 secreted (Fig. 2A). The secreted and 'non-secreted' proteins are listed in Table S2. Of the secreted proteins, 136 (81%) exhibited no change in abundance between Chow and HFD hepatocytes (Fig. 2B), while 30 proteins were increased and two were decreased in the HFD compared with Chow CM (Fig. 2C). A list of the differentially secreted proteins is presented in Figure 2D. Metacore was used to identify biological pathways associated with hepatocyte protein secretion differences mediated by steatosis. Enrichment analysis revealed an overrepresentation of secreted proteins associated with heme metabolism, cholesterol and sphingolipid transport, lipid metabolism and immune response (Fig. 2E). These processes are consistent with the important role of the liver in regulating metabolism and immune function.

Transcriptomic approaches do not accurately predict the hepatocyte protein secretion profile

We also performed global transcriptomic analysis of hepatocytes in parallel with the protein secretion studies with the aim of determining whether the protein secretome could be predicted by changes in transcript levels. In total, there were 45,281 probe sets on the chip, 15,835 probe sets were detected (Table S2), which corresponded to 11,526 unique transcripts. Of those unique transcripts, 533 genes were predicted to translate into secreted proteins based on bioinformatics profiling as described above. Of the genes corresponding to secreted

proteins, 418 (78%) exhibited no change in abundance between Chow and HFD hepatocytes, while 33 genes were up-regulated by HFD and 81 were down-regulated (Fig. 2F). To interpret these changes in a biological context, we analysed the differentially secreted genes using Metacore and identified a significant, biologically relevant association of these genes with the immune response and IGF-1 signaling. Hence, aside from the immune response, the bioinformatics approach did not predict enrichment of similar biological pathways when comparing the secreted protein or transcriptome data set. Consistent with this notion, the protein secretome was not predicted by changes in transcript levels (Fig. 2G) with only seven transcripts/proteins identified as upregulated in both analyses. These are apolipoprotein A, zinc-alpha-2-glycoprotein, inter-alpha-trypsin inhibitor heavy chain H2, insulin-like growth factor-binding protein 4, alpha-2-HS-glycoprotein, alpha-2-antiplasmin and hepatocyte growth factor activator. Thus, consistent with previous comparative analyses of the murine transcriptome and proteome (Ghazalpour et al., 2011), these data demonstrate that the protein secretome cannot be accurately predicted by assessing changes in the transcriptome obtained from the same biological source, thereby highlighting that post-transcriptional events impact significantly on the protein secretion profile in hepatocytes.

Fetuin B is increased in obese humans with liver steatosis

We next examined steatosis-regulated proteins for their involvement in glucose metabolism. Of the differentially secreted proteins, fetuin B was increased 1.5-fold in HFD compared with Chow hepatocytes based on iTRAQ mass spectrometry (Fig. 2D). This was confirmed by independent immunoblot experiments of the secreted culture medium (Fig. 3A, inset) and coincided with a 3-fold increase in hepatocyte fetuin B content (Fig. 3B). Fetuin-B shares 22% homology with fetuin A, a circulating glycoprotein that causes insulin resistance by activating toll-like receptors and inducing inflammatory signalling (Pal et al., 2012; Stefan and Haring, 2013a) and fetuin B levels have previously been associated with rodent obesity

(Choi et al., 2010). Accordingly, we examined plasma and liver fetuin B levels in obese humans without or with steatotic livers (steatosis/NAFLD) as determined from liver biopsy. The participants' characteristics are included in Table 1. Plasma fetuin B levels were increased in the obese participants with simple steatosis as compared to obese participants without steatosis (Fig. 3C). Liver fetuin B protein content was not different between groups (Fig. S3A-C). Plasma fetuin B was positively correlated with fasting insulin (Fig. S3D) and HOMA-IR, an index of insulin resistance (Fig. 3D), and did not correlate with body mass index (adiposity), the liver damage marker alanine aminotransferase, the inflammatory marker C-reactive protein or blood lipids including total cholesterol, HDL cholesterol, LDL cholesterol, triglycerides, and free fatty acids (Fig. S3E-L).

Fetuin B impairs insulin sensitivity in myotubes and hepatocytes

Examination of fetuin B in a second human cohort showed that plasma fetuin B levels were not increased in obese individuals without diabetes, but were increased in type 2 diabetes patients compared with lean, insulin sensitive individuals (Fig. 3E). This prompted us to examine the direct effect of fetuin B on glucose metabolism. Fetuin B decreased insulin-stimulated glucose uptake in myotubes (Fig. 3F) in a time and dose-dependent manner. Defects in insulin action only became evident after 24 h of fetuin B treatment (no effects at 30 min or 2 h, data not shown) and at fetuin B concentrations reported in human plasma (~300 μmol/L, Fig. S3M-O) (Denecke et al., 2003). Fetuin B also impaired insulin action in primary hepatocytes as demonstrated by impaired insulin-mediated suppression of the gluconeogenic genes *G6pc* (encoding glucose-6-phosphatase) and *Pck1* (encoding cytosolic phosphoenolpyruvate carboxykinase) (Fig. 3G-H), and tended to decrease (P=0.06) insulin-mediated Akt phosphorylation (Fig. 3I).

Fetuin B shares 22% homology with fetuin A, a circulating glycoprotein that causes insulin resistance by activating toll-like receptors and inducing inflammatory signalling (Pal et al., 2012; Stefan and Haring, 2013a). Accordingly, we determined whether fetuin B could exert similar effects. Fetuin B treatment had no effect on pro-inflammatory signaling (Fig. 3J) or cytokine release (Fig. 3K) from primary bone marrow-derived macrophages, which contrasted the actions of the canonical TLR4 ligand LPS. Pro-inflammatory signaling was similarly unaffected in myotubes as evidenced by similar phosphorylation of JNK ($p=0.69$) and ERK ($p=0.65$), and by similar contents of IκBα ($p=0.43$) (Fig. S4A-C). Consistent with these effects, plasma TNFα levels were not increased 2 h after fetuin B administration into lean mice (Fig. 3L). Hence, unlike fetuin A, physiological concentrations of fetuin B do not induce pro-inflammatory signaling.

Fetuin B causes glucose intolerance but not insulin resistance in mice

To study the effects of fetuin B on glucose metabolism *in vivo*, recombinant fetuin B was injected intraperitoneally into mice, and glucose tolerance was assessed 2 h later. Plasma fetuin B levels were increased 2 h after the fetuin B injection (Fig. 4A). Glucose tolerance was significantly impaired in mice treated with fetuin B (Fig. 4B) while plasma insulin levels were similar between fetuin B and control mice 15 min after glucose administration (Fig. 4C). Fetuin B administration did not affect insulin or AMP-activated protein kinase (AMPK) signalling in the liver (Fig. 4D) or skeletal muscle (not shown) during the glucose tolerance test.

Insulin-mediated effects account for ~50% of the glucose clearance during a glucose tolerance test (Ahren and Pacini, 2002; Alonso et al., 2012; Best et al., 1996). Accordingly, we directly assessed insulin sensitivity by performing hyperinsulinemic-euglycemic clamps in mice 2 h after i.p. fetuin B administration. Mice were clamped at 10.7 ± 0.2 mmol/l

glucose, and steady-state glucose levels were achieved in both groups. The glucose infusion rate required to maintain euglycemia was similar in both groups (Fig. 4E), indicating equivalent whole-body insulin sensitivity. Neither the suppression of hepatic glucose output (Fig. 4F) nor the glucose rate of disappearance (Fig. 4G) was different between treatment groups. Independent experiments examining insulin sensitivity during a short-term intravenous insulin tolerance test also showed no effect of fetuin B on whole-body or tissue-specific insulin action (Fig. S4D-F). Hence, fetuin B did not affect hepatic or peripheral insulin sensitivity.

Glucose effectiveness refers to the capacity for glucose to enhance peripheral glucose uptake and suppress endogenous glucose production independent of insulin, and it accounts for the remaining ~50% of the glucose clearance during a glucose tolerance test (Alonso et al., 2012; Best et al., 1996). Circulating plasma lactate levels increase in response to a glucose challenge due to a combination of tissue glucose uptake and glycolysis to form lactate, which is then released into the circulation. Decreased lactate production in the absence of any difference in insulin sensitivity has been linked to decreased glucose effectiveness (Best et al., 1996). Plasma lactate during a glucose challenge was decreased in mice pre-treated with fetuin B, suggestive of decreased glucose effectiveness in these mice (Fig. 4H).

Reducing fetuin B improves glucose tolerance in obese mice

To confirm the effect of Fetuin B on glucose metabolism in an independent experimental model, mice fed a high-fat diet for 6 weeks were injected with an adeno-associated virus (serotype 8) containing a shRNA against either fetuin B or a scrambled shRNA. Fetuin B shRNA decreased fetuin B expression in liver and plasma fetuin B by 33% and 72% compared with scramble shRNA (Fig. 4I-J). The silencing effects were not restricted to the liver with decreased fetuin B in white adipose tissue and heart of fetuin B shRNA treated

mice (Fig. S4G-H). The decrease in liver fetuin B was closely associated with changes in plasma fetuin B, supporting the premise that the liver is most likely a primary source of circulating fetuin B (Fig. 4K). Body mass was not impacted by fetuin B shRNA (Fig. 4L), while glucose tolerance was markedly improved in mice treated with fetuin B shRNA compared with littermates treated with shRNA control (Fig. 4M). Collectively, these data demonstrate improved whole-body glucose metabolism upon reduction of circulating fetuin B in obese mice.

Discussion

Hepatic steatosis is a common condition that is closely associated with obesity and type 2 diabetes. Clinical studies demonstrate that steatosis is more closely related to the development of insulin resistance than obesity *per se* (Fabbrini et al., 2009; Korenblat et al., 2008; Koska et al., 2008; Linder et al., 2014), indicating that signals originating from the steatotic liver might negatively affect insulin action via inter-tissue communication. We report that the hepatocyte protein secretion profile is altered by steatosis and that the combination of the hepatocyte secreted products causes insulin resistance and inflammation. We used this 'omics' platform to identify proteins whose secretion is upregulated by steatosis and focussed on fetuin B, a highly expressed liver protein that was previously reported to be upregulated in obese mice. We also provide evidence that fetuin B is a hepatokine that is regulated by steatosis in humans, is elevated in type 2 diabetes and causes glucose intolerance by modulating insulin-independent glucose metabolism.

Mapping of the murine liver identified ~7000 proteins of which 25% were also detected in the plasma (Lai et al., 2008), suggesting that the liver secretes many proteins to regulate systemic biological processes. The present studies have assessed the hepatocyte protein secretome and provide several important insights supporting further mechanistic studies.

First, we have identified 538 proteins in the hepatocyte secretion medium, with 168 assigned as classically secreted, thereby confirming the hepatocyte as a major producer of plasma proteins. As a comparison, adipocytes secrete ~160 proteins (Crowe et al., 2009) and given the involvement of adipokines in regulating metabolic phenotypes, these results implicate hepatokines as important regulators of biological processes. In addition, since two-thirds of the proteins identified in the conditioned medium do not contain a signal peptide, it is likely that significant protein secretion from the hepatocyte occurs through unconventional secretory processes. In unconventional secretion, proteins that lack a N-terminal signal peptide and do not get delivered to the lumen of the endoplasmic reticulum can be transported into the extracellular milieu via diverse pathways. These include transit across the plasma membrane independently of a cell surface transporter, secretory lysosome-mediated membrane fusion, plasma membrane budding, transport via exosomes produced in multivesicular bodies, secretory autophagy and release via mitochondrial derived vesicles (Zhang and Schekman, 2013). While the existence of unconventional secretion is widely accepted, targeted studies are required to delineate if, and how, specific proteins identified in our studies are secreted from hepatocytes.

Next, we have shown that diet-induced steatosis alters the hepatic protein secretion profile. The liver transcriptome and proteome is altered in mice fed a high-fat diet (Kirpich et al., 2010; Schmid et al., 2004) and in humans with steatosis (Greco et al., 2008; Younossi et al., 2005), and active protein synthesis in the endoplasmic reticulum (ER) is reduced in the livers of obese mice (Fu et al., 2012). These latter findings indicate altered protein secretion because the ER/Golgi-dependent secretory pathway exports the vast majority of secreted proteins. We extend on these observations in reporting that the hepatocyte secretome is sensitive to steatosis, with altered secretion in 20% of the classically secreted proteins. Bioinformatic analyses of the overall changes in protein secretion predicted alterations in

inflammation and metabolism, and cell-based studies confirmed that the secretome from the steatotic hepatocyte impaired insulin action in muscle and liver, and activated pro-inflammatory pathways in macrophages. It is noteworthy that more than half of the differentially secreted proteins in our studies are upregulated in the serum of type 2 diabetes patients (Kaur et al., 2012), suggesting that dysregulated hepatic protein secretion induced by steatosis might be an important component of diabetes development and that a subset of the protein secretome that we have identified as steatosis-responsive might predict diabetes development. Further work will be needed to delineate whether and how these proteins, either individually or in combination, contribute to the development of insulin resistance and other metabolic dysfunctions.

The utility of the proteomics approach is evidenced by the identification of fetuin B as a steatosis-responsive hepatokine that negatively impacts glucose metabolism. Fetuin B is a member of the cystatin superfamily of cysteine protease inhibitors and shares 22% homology with fetuin A (Denecke et al., 2003). Fetuin A (also known as alpha-2-HS-glycoprotein) is increased in patients with steatosis (Stefan et al., 2006); its circulating levels are negatively correlated with insulin sensitivity in humans (Mori et al., 2006), and insulin signalling is improved in *Ahsg*$^{-/-}$ (encoding fetuin A) mice (Mathews et al., 2002). Fetuin A induces metabolic dysfunction through a number of mechanisms that include inhibition of insulin receptor tyrosine kinase activity and the promotion of inflammation in immune cells and adipocytes (Stefan and Haring, 2013b). Recently, fetuin A was identified as an adaptor protein for saturated fatty acid induced activation of toll-like receptor 4 signaling, which promoted lipid-induced insulin resistance (Pal et al., 2012), and the fetuin A / FFA interaction appears to predict the development of insulin resistance in humans (Stefan and Haring, 2013a). Importantly, we show in this study that fetuin B acts in a manner quite distinct from that of fetuin A.

Previous studies have reported increased fetuin-B levels in obese rodents (Choi et al., 2010); however, the role of fetuin B in metabolic regulation and the clinical relevance of these observations were unknown. We report that fetuin B is increased in the plasma of type 2 diabetes patients and individuals with hepatic steatosis, and that plasma fetuin B levels are positively associated with insulin resistance. Fetuin B decreased insulin sensitivity in cultured muscle and hepatocytes when administered at physiological concentrations and did not activate proinflammatory signaling. In contrast, while fetuin B caused glucose intolerance in mice, it did not impair insulin signaling after glucose administration and did not reduce insulin sensitivity during hyperinsulinemic-euglycemic clamps in mice. While the findings in these different models appear somewhat discordant, they are not without explanation. Insulin resistance in humans develops over many years and the clamp studies in mice were conducted 2 h after fetuin B administration. Furthermore, the cell culture studies demonstrated that fetuin B effects on insulin action are both dose- and time-dependent (i.e. insulin resistance was evident after 24 h, but not 2 h) and we surmise that the relatively small (yet physiological) and transient (2 h) increase in i.p delivered fetuin B might have been insufficient to impair insulin action in mice *in vivo*.

Glucose disposal is controlled by the combined effects of insulin secretion, insulin sensitivity of peripheral tissues and glucose effectiveness, which refers to the ability of glucose to promote its own disposal, independently of insulin (Alonso et al., 2012; Best et al., 1996). Glucose effectiveness is at least as important as insulin for glucose clearance, accounting for ~50% of an oral glucose tolerance test in normal individuals and ~80% in obese, insulin-resistant individuals (Best et al., 1996). Similar contributions are reported for lean and obese mice (Alonso et al., 2012). Although glucose effectiveness was presumed to occur by the mass action of glucose to drive glucose into cells in a gradient-dependent manner, it is now clear that this process is regulated. For example, glucose effectiveness is suppressed by ~50%

in non-obese men with impaired glucose tolerance and type 2 diabetes patients (Best et al., 1996), and glucose effectiveness can be enhanced by exercise training in humans (Nishida et al., 2001) and in mice by FGF19 acting through the central nervous system (Morton et al., 2013). While a large body of physiological and clinical data has described the existence and regulation of glucose effectiveness, the underlying cellular and molecular process are currently unknown. In the liver, glucoregulatory hormones such as glucagon and cortisol impair glucose effectiveness, as do chronically elevated FFA levels (Tonelli et al., 2005). While peripheral glucose effectiveness (e.g. muscle) is the dominant component of whole-body glucose effectiveness (Mevorach et al., 1998), its molecular regulation is largely unknown (Tonelli et al., 2005).

Our *in vivo* studies in mice demonstrate that fetuin B causes glucose intolerance in lean mice, independent of changes in plasma insulin and insulin signal transduction during glucose administration, or changes in insulin sensitivity during clamps. Rather, our studies suggest that glucose effectiveness is reduced by fetuin B. In support of this conclusion, fetuin B reduced plasma lactate levels during a glucose challenge, which is consistent with previous studies reporting reduced glycolysis of glucose to lactate and impaired glucose effectiveness in *ob/ob* mice (Morton et al., 2013). While we do not know the mechanism of action for fetuin B, we can conclude that fetuin B does not impact several putative regulators of glucose effectiveness or insulin action including proinflammatory signaling (Fig. 3J/K), adipocyte lipolysis (Fig. S4I-J), fatty acid metabolism in myotubes (Fig. S4K) and hepatocytes (Fig. S4L) or AMPK signalling in skeletal muscle and liver (Fig. S4M). Despite this limitation, the data establish a model whereby fetuin B secretion from the liver is increased by steatosis and diminishes glucose lowering through insulin-independent mechanisms. Furthermore, partial silencing of fetuin B improved glucose tolerance in obese mice, independent of weight loss, suggesting a role for fetuin B in the pathogenesis of diabetes.

In conclusion, these data provide a comprehensive examination of the hepatocyte protein secretome and demonstrate marked changes in response to simple steatosis, a metabolic abnormality that is common in type 2 diabetes and dyslipidemia. Conceptually, our work extends on understanding the pathogenesis of diabetes by demonstrating that the combined secreted products from the steatotic hepatocyte are proinflammatory and promote insulin resistance. The identification of fetuin B as a steatosis-responsive hepatokine that induces dysregulated glucose metabolism demonstrates the utility of this approach and paves the way for validating other molecules that could be important in the pathogenesis of diabetes and cardiovascular disease.

Experimental procedures

Additional procedures can be found in the *Supplemental Experimental Procedures*.

Human studies were approved by the medical ethical committee of Maastricht University and the Alfred Hospital human research ethics committee. All participants provided written informed consent before participation in the studies. In one cohort, a fasted plasma sample was obtained before surgery and a liver biopsy was taken during surgery to assess the presence of liver steatosis according to the Brunt classification (Brunt et al., 1999). The healthy group (n=14) comprised patients with <5% steatotic hepatocytes (score 0). The steatotic group (n=11) comprised patients with >5% steatotic hepatocytes (score 1-3) without significant inflammation as observed after H&E staining (i.e. no intra-acinar inflammatory foci per 20 fields with a 20 ocular and no portal tract inflammation). In the second cohort, venous blood samples were obtained from an antecubital vein after an overnight fast in 28 males who were lean insulin-sensitive (n=9), obese insulin-sensitive (n=5) and obese with type 2 diabetes (n=14). Detailed study protocols are outlined in the supplementary methods.

Animal studies were approved by the Monash University School of Biomedical Science Animal Ethics Committee. Male C57BL/6 mice aged 8 weeks were fed either a chow (4.6% fat) or high fat diet (36% fat,) for 6 weeks prior to hepatocyte isolation, which was performed as described in the supplementary methods. Mice were fasted for 4 h from 0700 h then injected i.p with fetuin B (1 μg/g body mass) (Life research) 2 h prior to glucose tolerance tests (2 g/kg D-glucose), insulin tolerance tests (1U/kg) or hyperinsulinemic-euglycemic clamps (4 mU/kg/min) as described (Borg et al., 2014; Mason et al., 2014). In separate experiments, mice were fed a HFD for 6 weeks. After one week, an adenoassociated virus serotype 8 (AAV8) driven by a CMV promoter ($1x10^{12}$gc), containing an shRNA sequence

specific for murine fetuin B (Vector Biolabs, shADV-259329) was injected via the tail vein. Control mice were injected with the same vector containing LacZ.

Cell culture was performed in L6 GLUT4myc myotubes, primary murine hepatocytes and bone marrow derived macrophages. Primary hepatocytes were obtained from anaesthetized (3% isofluorane) mice by inserting a 24 gauge catheter into the hepatic portal vein and perfusing with Hanks Buffered Salt Solution and collagenase buffer (Liberase TM Research Grade, 50 μg/ml, Roche) in series. Conditioned media was collected in EX-CELL® 325 Protein-Free CHO Serum-Free Medium (SAFC Biosciences) for 24 h, then placed on cells for 16 h prior to functional analyses. Fetuin B was purchased from Life Research. Detailed protocols of functional assays are outlined in the Supplementary Methods.

iTRAQ sample preparation and data acquisition. In short, proteins were reduced with TCEP, alkylated with MMTS, digested with trypsin and labelled with iTRAQ 8-plex reagents following the manufacturer's instructions. The iTRAQ labeled samples were combined in equal ratios, fractionated using SCX and analysed by reversed phase nanoLC ESI MS/MS using a Top 10 data dependent acquisition strategy with a 5600 TripleTOF mass spectrometer. See Supplementary methods for detailed procedures.

Flow cytometry. Cells were analysed using LSR II (BD Biosciences) and data analysis was completed using Flowjo cytometric analysis program (version 10).

Transcriptomics Mouse amplified RNA quality was ascertained on the Agilent Bioanalyser 2100 using the NanoChip protocol. 750 ngs of amplified RNA was hybridized to the *Ilumina Mouse WG-6 v2 Expression BeadChip* the chip was washed then coupled with Cy3 and

scanned in the Illumina iScan Reader. Genes with an expression difference of ≥ 1.20-fold with 95% confidence interval between the conditions were considered to be different.

All biochemical measures, blood chemistry, immunoblotting, qRT-PCR, immuno-histochemistry were performed by standard approaches and are detailed in the supplementary methods.

Statistical analysis

Statistical analysis was performed using paired or unpaired Student's t-tests, one- or two-way analysis of variance (ANOVA) or repeated measures ANOVA where appropriate. Individual means were compared using a Bonferroni post hoc analysis when required. Statistical significance was set *a priori* at $P \leq 0.05$. Data are reported as means ± SEM.

Author contributions

Conceived and designed the experiments: RCM, AJH, MJW. Performed the experiments: RCM, AM, RB, SSR, JWG, JCYL, GIL, MJK, MM, CRB, MJW. Analyzed the data: RCM, AJH, AM, MB, JCYL, RJAG, MJK, GIL, MJW. Wrote the paper: RCR, MJW. Edited the manuscript: AJH, AM, MB, JCYL, RJAG, BAK, MJK, MAF, SSR, MM, GIL, CRB.

Acknowledgements

We acknowledge the technical assistance of Xiaomin Song, Dana Pascovici and Thiri Zaw (Australian Proteome Analysis Facility) and Michael de Veer (Monash University). This work was supported by research grants from the National Health and Medical Research Council of Australia (NHMRC, ID: 1061278), Diabetes Australia Research Trust (MJW) and Monash University (MJW) and fellowships from the National Health and Medical Research

Council of Australia (AJH ID: 606766; MAF ID: APP1021168, BK ID: 1059454; MJW ID: 606460 & 1077703).

References

Abdul-Ghani, M.A., Matsuda, M., and DeFronzo, R.A. (2008). Strong association between insulin resistance in liver and skeletal muscle in non-diabetic subjects. Diabet Med *25*, 1289-1294.

Ahren, B., and Pacini, G. (2002). Insufficient islet compensation to insulin resistance vs. reduced glucose effectiveness in glucose-intolerant mice. Am J Physiol Endocrinol Metab *283*, E738-744.

Alonso, L.C., Watanabe, Y., Stefanovski, D., Lee, E.J., Singamsetty, S., Romano, L.C., Zou, B., Garcia-Ocana, A., Bergman, R.N., and O'Donnell, C.P. (2012). Simultaneous measurement of insulin sensitivity, insulin secretion, and the disposition index in conscious unhandled mice. Obesity (Silver Spring) *20*, 1403-1412.

Bellentani, S., Saccoccio, G., Masutti, F., Croce, L.S., Brandi, G., Sasso, F., Cristanini, G., and Tiribelli, C. (2000). Prevalence of and risk factors for hepatic steatosis in Northern Italy. Annals of internal medicine *132*, 112-117.

Best, J.D., Kahn, S.E., Ader, M., Watanabe, R.M., Ni, T.C., and Bergman, R.N. (1996). Role of glucose effectiveness in the determination of glucose tolerance. Diabetes Care *19*, 1018-1030.

Borg, M.L., Lemus, M., Reichenbach, A., Selathurai, A., Oldfield, B.J., Andrews, Z.B., and Watt, M.J. (2014). Hypothalamic neurogenesis is not required for the improved insulin sensitivity following exercise training. Diabetes.

Browning, J.D., Szczepaniak, L.S., Dobbins, R., Nuremberg, P., Horton, J.D., Cohen, J.C., Grundy, S.M., and Hobbs, H.H. (2004). Prevalence of hepatic steatosis in an urban population in the United States: impact of ethnicity. Hepatology *40*, 1387-1395.

Brunt, E.M., Janney, C.G., Di Bisceglie, A.M., Neuschwander-Tetri, B.A., and Bacon, B.R. (1999). Nonalcoholic steatohepatitis: a proposal for grading and staging the histological lesions. Am J Gastroenterol *94*, 2467-2474.

Chitturi, S., Farrell, G.C., and George, J. (2004). Non-alcoholic steatohepatitis in the Asia-Pacific region: future shock? J Gastroenterol Hepatol *19*, 368-374.

Choi, J.W., Wang, X., Joo, J.I., Kim, D.H., Oh, T.S., Choi, D.K., and Yun, J.W. (2010). Plasma proteome analysis in diet-induced obesity-prone and obesity-resistant rats. Proteomics *10*, 4386-4400.

Crowe, S., Wu, L.E., Economou, C., Turpin, S.M., Matzaris, M., Hoehn, K.L., Hevener, A.L., James, D.E., Duh, E.J., and Watt, M.J. (2009). Pigment epithelium-derived factor contributes to insulin resistance in obesity. Cell Metab *10*, 40-47.

Day, C.P., and James, O.F. (1998). Steatohepatitis: a tale of two "hits"? Gastroenterology *114*, 842-845.

Denecke, B., Graber, S., Schafer, C., Heiss, A., Woltje, M., and Jahnen-Dechent, W. (2003). Tissue distribution and activity testing suggest a similar but not identical function of fetuin-B and fetuin-A. The Biochemical journal *376*, 135-145.

Fabbrini, E., Magkos, F., Mohammed, B.S., Pietka, T., Abumrad, N.A., Patterson, B.W., Okunade, A., and Klein, S. (2009). Intrahepatic fat, not visceral fat, is linked with metabolic complications of obesity. Proc Natl Acad Sci U S A *106*, 15430-15435.

Fu, S., Fan, J., Blanco, J., Gimenez-Cassina, A., Danial, N.N., Watkins, S.M., and Hotamisligil, G.S. (2012). Polysome profiling in liver identifies dynamic regulation of endoplasmic reticulum translatome by obesity and fasting. PLoS Genet *8*, e1002902.

Ghazalpour, A., Bennett, B., Petyuk, V.A., Orozco, L., Hagopian, R., Mungrue, I.N., Farber, C.R., Sinsheimer, J., Kang, H.M., Furlotte, N., et al. (2011). Comparative analysis of proteome and transcriptome variation in mouse. PLoS Genet *7*, e1001393.

Greco, D., Kotronen, A., Westerbacka, J., Puig, O., Arkkila, P., Kiviluoto, T., Laitinen, S., Kolak, M., Fisher, R.M., Hamsten, A., et al. (2008). Gene expression in human NAFLD. Am J Physiol Gastrointest Liver Physiol *294*, G1281-1287.

Kaur, P., Rizk, N.M., Ibrahim, S., Younes, N., Uppal, A., Dennis, K., Karve, T., Blakeslee, K., Kwagyan, J., Zirie, M., et al. (2012). iTRAQ-based quantitative protein expression profiling and MRM verification of markers in type 2 diabetes. Journal of proteome research *11*, 5527-5539.

Kharitonenkov, A., Shiyanova, T.L., Koester, A., Ford, A.M., Micanovic, R., Galbreath, E.J., Sandusky, G.E., Hammond, L.J., Moyers, J.S., Owens, R.A., et al. (2005). FGF-21 as a novel metabolic regulator. J Clin Invest *115*, 1627-1635.

Kirpich, I.A., Gobejishvili, L.N., Homme, M.B., Waigel, S., Cave, M., Arteel, G., Barve, S.S., McClain, C.J., and Deaciuc, I.V. (2010). Integrated hepatic transcriptome and proteome analysis of mice with high-fat diet-induced nonalcoholic fatty liver disease. J Nutr Biochem.

Korenblat, K.M., Fabbrini, E., Mohammed, B.S., and Klein, S. (2008). Liver, muscle, and adipose tissue insulin action is directly related to intrahepatic triglyceride content in obese subjects. Gastroenterology *134*, 1369-1375.

Koska, J., Stefan, N., Permana, P.A., Weyer, C., Sonoda, M., Bogardus, C., Smith, S.R., Joanisse, D.R., Funahashi, T., Krakoff, J., et al. (2008). Increased fat accumulation in liver may link insulin resistance with subcutaneous abdominal adipocyte enlargement, visceral adiposity, and hypoadiponectinemia in obese individuals. Am J Clin Nutr *87*, 295-302.

Kraegen, E.W., Clark, P.W., Jenkins, A.B., Daley, E.A., Chisholm, D.J., and Storlien, L.H. (1991). Development of muscle insulin resistance after liver insulin resistance in high-fat-fed rats. Diabetes *40*, 1397-1403.

Kumar, K.G., Trevaskis, J.L., Lam, D.D., Sutton, G.M., Koza, R.A., Chouljenko, V.N., Kousoulas, K.G., Rogers, P.M., Kesterson, R.A., Thearle, M., et al. (2008). Identification of adropin as a secreted factor linking dietary macronutrient intake with energy homeostasis and lipid metabolism. Cell Metab *8*, 468-481.

Lai, K.K., Kolippakkam, D., and Beretta, L. (2008). Comprehensive and quantitative proteome profiling of the mouse liver and plasma. Hepatology *47*, 1043-1051.

Larson-Meyer, D.E., Newcomer, B.R., Ravussin, E., Volaufova, J., Bennett, B., Chalew, S., Cefalu, W.T., and Sothern, M. (2011). Intrahepatic and intramyocellular lipids are determinants of insulin resistance in prepubertal children. Diabetologia *54*, 869-875.

Linder, K., Springer, F., Machann, J., Schick, F., Fritsche, A., Haring, H.U., Blumenstock, G., Ranke, M.B., Stefan, N., Binder, G., et al. (2014). Relationships of body composition and liver fat content with insulin resistance in obesity-matched adolescents and adults. Obesity (Silver Spring) *22*, 1325-1331.

Mason, R.R., Mokhtar, R., Matzaris, M., Selathurai, A., Kowalski, G.M., Mokbel, N., Meikle, P.J., Bruce, C.R., and Watt, M.J. (2014). PLIN5 deletion remodels intracellular lipid composition and causes insulin resistance in muscle. Molecular metabolism *3*, 652-663.

Mathews, S.T., Singh, G.P., Ranalletta, M., Cintron, V.J., Qiang, X., Goustin, A.S., Jen, K.L., Charron, M.J., Jahnen-Dechent, W., and Grunberger, G. (2002). Improved insulin sensitivity and resistance to weight gain in mice null for the Ahsg gene. Diabetes *51*, 2450-2458.

Mevorach, M., Giacca, A., Aharon, Y., Hawkins, M., Shamoon, H., and Rossetti, L. (1998). Regulation of endogenous glucose production by glucose per se is impaired in type 2 diabetes mellitus. J Clin Invest *102*, 744-753.

Misu, H., Takamura, T., Takayama, H., Hayashi, H., Matsuzawa-Nagata, N., Kurita, S., Ishikura, K., Ando, H., Takeshita, Y., Ota, T., et al. (2010). A liver-derived secretory protein, selenoprotein P, causes insulin resistance. Cell metabolism *12*, 483-495.

Mori, K., Emoto, M., Yokoyama, H., Araki, T., Teramura, M., Koyama, H., Shoji, T., Inaba, M., and Nishizawa, Y. (2006). Association of serum fetuin-A with insulin resistance in type 2 diabetic and nondiabetic subjects. Diabetes Care *29*, 468.

Morton, G.J., Matsen, M.E., Bracy, D.P., Meek, T.H., Nguyen, H.T., Stefanovski, D., Bergman, R.N., Wasserman, D.H., and Schwartz, M.W. (2013). FGF19 action in the brain induces insulin-independent glucose lowering. J Clin Invest *123*, 4799-4808.

Nishida, Y., Higaki, Y., Tokuyama, K., Fujimi, K., Kiyonaga, A., Shindo, M., Sato, Y., and Tanaka, H. (2001). Effect of mild exercise training on glucose effectiveness in healthy men. Diabetes Care *24*, 1008-1013.

Oike, Y., Akao, M., Yasunaga, K., Yamauchi, T., Morisada, T., Ito, Y., Urano, T., Kimura, Y., Kubota, Y., Maekawa, H., et al. (2005). Angiopoietin-related growth factor antagonizes obesity and insulin resistance. Nat Med *11*, 400-408.

Pal, D., Dasgupta, S., Kundu, R., Maitra, S., Das, G., Mukhopadhyay, S., Ray, S., Majumdar, S.S., and Bhattacharya, S. (2012). Fetuin-A acts as an endogenous ligand of TLR4 to promote lipid-induced insulin resistance. Nature medicine *18*, 1279-1285.

Petersen, K.F., Dufour, S., Befroy, D., Lehrke, M., Hendler, R.E., and Shulman, G.I. (2005). Reversal of nonalcoholic hepatic steatosis, hepatic insulin resistance, and hyperglycemia by moderate weight reduction in patients with type 2 diabetes. Diabetes *54*, 603-608.

Samuel, V.T., and Shulman, G.I. (2012). Mechanisms for insulin resistance: common threads and missing links. Cell *148*, 852-871.

Schmid, G.M., Converset, V., Walter, N., Sennitt, M.V., Leung, K.Y., Byers, H., Ward, M., Hochstrasser, D.F., Cawthorne, M.A., and Sanchez, J.C. (2004). Effect of high-fat diet on the expression of proteins in muscle, adipose tissues, and liver of C57BL/6 mice. Proteomics *4*, 2270-2282.

Stefan, N., and Haring, H.U. (2013a). Circulating fetuin-A and free fatty acids interact to predict insulin resistance in humans. Nat Med *19*, 394-395.

Stefan, N., and Haring, H.U. (2013b). The role of hepatokines in metabolism. Nat Rev Endocrinol *9*, 144-152.

Stefan, N., Hennige, A.M., Staiger, H., Machann, J., Schick, F., Krober, S.M., Machicao, F., Fritsche, A., and Haring, H.U. (2006). Alpha2-Heremans-Schmid glycoprotein/fetuin-A is associated with insulin resistance and fat accumulation in the liver in humans. Diabetes Care *29*, 853-857.

Stewart, L.K., Wang, Z., Ribnicky, D., Soileau, J.L., Cefalu, W.T., and Gettys, T.W. (2009). Failure of dietary quercetin to alter the temporal progression of insulin resistance among tissues of C57BL/6J mice during the development of diet-induced obesity. Diabetologia *52*, 514-523.

Strissel, K.J., Stancheva, Z., Miyoshi, H., Perfield, J.W., 2nd, DeFuria, J., Jick, Z., Greenberg, A.S., and Obin, M.S. (2007). Adipocyte death, adipose tissue remodeling, and obesity complications. Diabetes *56*, 2910-2918.

Tonelli, J., Kishore, P., Lee, D.E., and Hawkins, M. (2005). The regulation of glucose effectiveness: how glucose modulates its own production. Curr Opin Clin Nutr Metab Care *8*, 450-456.

Toye, A.A., Dumas, M.E., Blancher, C., Rothwell, A.R., Fearnside, J.F., Wilder, S.P., Bihoreau, M.T., Cloarec, O., Azzouzi, I., Young, S., et al. (2007). Subtle metabolic and liver gene transcriptional changes underlie diet-induced fatty liver susceptibility in insulin-resistant mice. Diabetologia *50*, 1867-1879.

Turner, N., Kowalski, G.M., Leslie, S.J., Risis, S., Yang, C., Lee-Young, R.S., Babb, J.R., Meikle, P.J., Lancaster, G.I., Henstridge, D.C., et al. (2013). Distinct patterns of tissue-specific lipid accumulation during the induction of insulin resistance in mice by high-fat feeding. Diabetologia *56*, 1638-1648.

Wicklow, B.A., Wittmeier, K.D., MacIntosh, A.C., Sellers, E.A., Ryner, L., Serrai, H., Dean, H.J., and McGavock, J.M. (2012). Metabolic consequences of hepatic steatosis in overweight and obese adolescents. Diabetes care *35*, 905-910.

Xu, H., Barnes, G.T., Yang, Q., Tan, G., Yang, D., Chou, C.J., Sole, J., Nichols, A., Ross, J.S., Tartaglia, L.A., et al. (2003). Chronic inflammation in fat plays a crucial role in the development of obesity-related insulin resistance. J Clin Invest *112*, 1821-1830.

Younossi, Z.M., Baranova, A., Ziegler, K., Del Giacco, L., Schlauch, K., Born, T.L., Elariny, H., Gorreta, F., VanMeter, A., Younoszai, A., et al. (2005). A genomic and proteomic study of the spectrum of nonalcoholic fatty liver disease. Hepatology *42*, 665-674.

Zhang, M., and Schekman, R. (2013). Cell biology. Unconventional secretion, unconventional solutions. Science *340*, 559-561.

Zhang, X., Yang, J., Guo, Y., Ye, H., Yu, C., Xu, C., Xu, L., Wu, S., Sun, W., Wei, H., et al. (2010). Functional proteomic analysis of nonalcoholic fatty liver disease in rat models: enoyl-coenzyme a hydratase down-regulation exacerbates hepatic steatosis. Hepatology *51*, 1190-1199.

Figure legends

Figure 1: Steatotic hepatocytes secrete factors that cause insulin resistance and promote pro-inflammatory signaling.

C57Bl/6J mice were fed a chow or high-fat diet (HFD) for six weeks. Hepatocytes were isolated and the secreted products were collected.

(A) Purity of the hepatocyte isolation as shown by fluorescence-activated cell sorting analysis using a FITC-conjugated anti-albumin antibody.

(B) Immunofluorescence immunohistochemistry for CD45 (leukocytes), CD31 (endothelial cells) and F4/80 (macrophages) in cultured isolated hepatocytes. Inset, no primary antibody negative control. Quantification of cells positive for CD45 and F4/80 (macrophages) and CD31 is shown to the right. Isolated cells were cultured for 24 h and trypsinized before flow cytometry (n=3 independent donor mice). Scale bar = 25 μm.

(C) Nile Red staining showing increased neutral lipid accumulation in hepatocytes isolated from Chow vs. HFD mice. Scale bar = 50 μm (n=1 biological replicate).

(D) Biochemical determination of triglyceride (TAG) content in cultured hepatocytes. (n=8 biological replicates per group). *P<0.05 vs Chow.

(E) Pro-inflammatory signalling in hepatocytes was similar between both groups as measured by phosphorylation of JNK and expression of IkBα. (n=3 biological replicates with each containing 4 technical replicates per group).

L6-GLUT4myc myotubes or bone marrow-derived macrophages were incubated for 16 h in conditioned medium (CM) collected from the isolated hepatocyte of Chow or HFD mice.

(F) 2-deoxyglucose (2-DG) uptake in L6-GLUT4myc myotubes without (Control) or with 1 nM insulin. (n=3 biological replicates with each containing 3-4 technical replicates per group). *P<0.05 vs Chow CM, #P<0.05 vs. Control within the same treatment.

(G) Fatty acid metabolism in L6-GLUT4myc myotubes. (n=3 biological replicates with each containing 10 technical replicates per group). *P<0.05 vs. Chow CM.

(H) Bone marrow-derived macrophages (BMDM) macrophages pre-treated in CM were incubated in LPS at the indicated concentrations for 30 min. Left: pJNK/B-actin and Right: pIKK/B-actin. (n= 3 biological replicates, each performed with 3 technical replicates). *P<0.05 vs Chow CM.

All data are means ± SEM.

Figure 2: The hepatocyte protein secretome is altered with steatosis.

(A) Proteins detected in the hepatocyte conditioned medium of Chow and HFD hepatocytes. Secreted proteins are considered those with a N-terminal signal sequence or annotated as secreted in UniProt (keywords: GOCC or subcellular location). (n=8 biological replicates performed in 2 independent analytical experiments).

(B) Secreted proteins that are significantly different between Chow and HFD conditioned medium. (n=8 biological replicates performed in 2 independent experiments).

(C) Direction of change of proteins that are differentially secreted. (n=8 biological replicates performed in 2 independent experiments).

(D) List of differentially secreted proteins in Chow and HFD conditioned medium.

(E) Enrichment analysis highlighting the top biological processes represented in the protein secretome of HFD CM. Enrichment analysis was performed against mouse proteins defined as secreted in the Uniprot database.

(F) Representation of the cDNA microarray analysis from Chow and HFD hepatocytes.

(G) Overlap between the differentially secreted proteins (from iTRAQ) and the predicted differentially 'secreted' proteins using transcriptomics. Only seven genes/proteins were detected and changed in the same direction using both approaches. (n=8 biological replicates per group).

Figure 3: Fetuin B is upregulated in individuals with steatosis and type 2 diabetes and causes insulin resistance, but not inflammation, in cultured cells.

(A) Secreted fetuin B determined by immunoblot in the conditioned medium (n=4 per group from independent donor mice). *P<0.05 vs. Chow CM. A representative immunoblot of fetuin B in the conditioned medium is shown above (left: Chow CM, right: HFD CM). Equal loading was confirmed by imaging the stain free gel.

(B) Fetuin B protein expression in isolated hepatocytes (n=6 per group obtained from independent donor mice). *P<0.05 vs. Chow. A representative immunoblot is shown above (left: Chow, right: HFD). Blot normalized to total protein loading for each sample, which was obtained by visualization and quantification of the stain-free blot image.

(C) Plasma fetuin B levels in obese humans without (No Steatosis, n=14) or with liver steatosis (Steatosis, n=11). *P<0.05 vs. No Steatosis.

(D) Correlation between plasma fetuin B and HOMA-IR. n=21.

(E) Plasma fetuin B levels in individuals who were lean insulin-sensitive (n=9), obese insulin-sensitive (n=5), or obese with type 2 diabetes (n=14). *P<0.05 vs. Lean.

(F) 2-Deoxyglucose uptake in L6-GLUT4myc myotubes exposed to various concentrations of fetuin B for 24 h. (n=5 per group from 2 independent experiments). *P<0.05 vs. basal at the same fetuin B concentration.

(G) *Glc-6-p* and **(H)** *Pepck* expression in primary murine hepatocytes treated with fetuin B. Hepatocytes were incubated without (basal) or with 1 nM insulin for 2 h before RNA extraction. (n=3 biological replicates, each performed with 3-4 technical replicates). *P<0.05, main treatment effect (fetuin B).

(I) Phosphorylated Akt(Ser473) during insulin stimulation (1 nM) in primary murine hepatocytes. Representative immunoblot shown to the right. (n=3 biological replicates, each performed with 4 technical replicates).

(J) BMDM were treated with 150 μM fetuin B or 100 ng/ml LPS for the indicated time points. Phosphorylated JNK (T183/Y185) / JNK and IκBα / tubulin content determined by immunoblot. n=3 per condition from 1 experiment.

(K) BMDM were treated for 24 h with either LPS or fetuin B for 24 h at the indicated concentrations. TNFα and IL-1β concentrations in the culture media was assessed by ELISA. (n=3 per condition from 1 experiment).

(L) Mice were injected with recombinant fetuin B or control two hours prior to glucose administration (2g/kg) (n=5 per group). Plasma TNFα was measured 15 min after glucose administration.

All data are means ± SEM.

Figure 4. Fetuin B causes glucose intolerance in mice.

(A) Plasma fetuin B levels in mice 2 h after injection of recombinant fetuin B or control (n=4 per group). *P<0.05 vs. Control.

(B) Glucose tolerance test (2 g/kg) in C57Bl/6J mice treated without or with fetuin B 2 h prior to testing (n=7 Control, n=8 fetuin B). P<0.0001, main effect for fetuin B.

(C) Plasma insulin at 15 min of the glucose tolerance test (n=4 per group).

Mice were injected i.p with fetuin B 2h prior to hyperinsulinemic-euglycemic clamp.

(D) Insulin and AMPK signaling are unaffected by fetuin B administration during the glucose tolerance test. Mice were injected with fetuin B (F) or control (C) two hours prior to glucose administration. Tissues were freeze-clamped 15 min after glucose administration (2 g/kg). IR, insulin receptor; IRS, insulin receptor substrate; ACC, acetyl CoA carboxylase; AMPK, AMP-activated protein kinase. Representative blots of n=8 per group.

(E) Glucose infusion rate (GIR) during the clamp. Steady state GIR is denoted by the grey shading. **(F)** Suppression of hepatic glucose output by insulin. **(G)** Insulin-stimulated whole body glucose rate of disappearance (Rd). (n=7 Control, n=8 fetuin B).

(H) Plasma lactate during glucose tolerance test (2 g/kg) (n=5 per group).

(I-M) C57Bl/6J mice were fed a high-fat diet for 6 weeks and treated with adeno-associated virus containing a shRNA fetuin B or scramble shRNA for 5 weeks prior to experiments. **(I)** Liver fetuin B content and **(J)** plasma fetuin B levels in mice. **(K)** Correlation between liver fetuin B and plasma fetuin B **(L)** Body mass of mice before and after AAV administration. **(M)** Glucose tolerance tests in mice (2 mg/kg). For all experiments, (n=10 Control, n=6 fetuin B). *P<0.05 vs shNeg.

All data are means ± SEM.

Supplementary Data

Table S1. Top 50 proteins identified by iTRAQ

Accession	Name	Peptides	Location
sp|P07724|ALBU_MOUSE	Serum albumin OS=Mus musculus GN=Alb PE=1 SV=3	145	Secreted
sp|Q06890|CLUS_MOUSE	Clusterin OS=Mus musculus GN=Clu PE=1 SV=1	90	Secreted
sp|P02762|MUP6_MOUSE	Major urinary protein 6 OS=Mus musculus GN=Mup6 PE=1 SV=2	86	Secreted
sp|P11589|MUP2_MOUSE	Major urinary protein 2 OS=Mus musculus GN=Mup2 PE=1 SV=1	85	Secreted
sp|P11588|MUP1_MOUSE	Major urinary protein 1 OS=Mus musculus GN=Mup1 PE=1 SV=1	81	Secreted
sp|Q921I1|TRFE_MOUSE	Serotransferrin OS=Mus musculus GN=Tf PE=1 SV=1	75	Secreted
sp|P56480|ATPB_MOUSE	ATP synthase subunit beta, mitochondrial OS=Mus musculus GN=Atp5b PE=1 SV=2	48	Mito
sp|P10493|NID1_MOUSE	Nidogen-1 OS=Mus musculus GN=Nid1 PE=1 SV=1	44	Secreted
sp|P26443|DHE3_MOUSE	Glutamate dehydrogenase 1, mitochondrial OS=Mus musculus GN=Glud1 PE=1 SV=1	42	Mito
sp|Q8C196|CPSM_MOUSE	Carbamoyl-phosphate synthase [ammonia], mitochondrial OS=Mus musculus GN=Cps1 PE=1 SV=2	41	Mito
sp|P21614|VTDB_MOUSE	Vitamin D-binding protein OS=Mus musculus GN=Gc PE=1 SV=2	40	Secreted
sp|P63038|CH60_MOUSE	60 kDa heat shock protein, mitochondrial OS=Mus musculus GN=Hspd1 PE=1 SV=1	36	Mito
sp|P01027|CO3_MOUSE	Complement C3 OS=Mus musculus GN=C3 PE=1 SV=2	36	Secreted
sp|P20029|GRP78_MOUSE	78 kDa glucose-regulated protein OS=Mus musculus GN=Hspa5 PE=1 SV=3	35	ER
sp|P05202|AATM_MOUSE	Aspartate aminotransferase, mitochondrial OS=Mus musculus GN=Got2 PE=1 SV=1	34	Mito
sp|P63260|ACTG_MOUSE	Actin, cytoplasmic 2 OS=Mus musculus GN=Actg1 PE=1 SV=1	32	Cytoplasmic
sp|P24270|CATA_MOUSE	Catalase OS=Mus musculus GN=Cat PE=1 SV=3	29	Secreted
sp|Q61147|CERU_MOUSE	Ceruloplasmin OS=Mus musculus GN=Cp PE=1 SV=2	29	Secreted
sp|Q9DBT9|M2GD_MOUSE	Dimethylglycine dehydrogenase, mitochondrial OS=Mus musculus GN=Dmgdh PE=1 SV=1	28	Mito
sp|P63017|HSP7C_MOUSE	Heat shock cognate 71 kDa protein OS=Mus musculus GN=Hspa8 PE=1 SV=1	27	Cytoplasmic
sp|P11725|OTC_MOUSE	Ornithine carbamoyltransferase, mitochondrial OS=Mus musculus GN=Otc PE=1 SV=1	27	Mito
sp|P29699|FETUA_MOUSE	Alpha-2-HS-glycoprotein OS=Mus musculus GN=Ahsg PE=1 SV=1	27	Secreted
sp|P08226|APOE_MOUSE	Apolipoprotein E OS=Mus musculus GN=Apoe PE=1 SV=2	27	Secreted
sp|Q63880|EST31_MOUSE	Liver carboxylesterase 31 OS=Mus musculus GN=Es31 PE=1 SV=2	27	Secreted
sp|P09103|PDIA1_MOUSE	Protein disulfide-isomerase OS=Mus musculus GN=P4hb PE=1 SV=1	25	ER
sp|P08249|MDHM_MOUSE	Malate dehydrogenase, mitochondrial OS=Mus musculus GN=Mdh2 PE=1 SV=3	24	Mito
sp|Q8VCT4|CES3_MOUSE	Carboxylesterase 3 OS=Mus musculus GN=Ces3 PE=1 SV=1	24	Secreted
sp|P27773|PDIA3_MOUSE	Protein disulfide-isomerase A3 OS=Mus musculus GN=Pdia3 PE=1 SV=2	22	ER
sp|Q8VCU1|ES31L_MOUSE	Liver carboxylesterase 31-like OS=Mus musculus GN=Gm4738 PE=2 SV=1	22	Secreted
sp|P07759|SPA3K_MOUSE	Serine protease inhibitor A3K OS=Mus musculus GN=Serpina3k PE=1 SV=2	21	Secreted
sp|Q91Y97|ALDOB_MOUSE	Fructose-bisphosphate aldolase B OS=Mus musculus GN=Aldob PE=1 SV=3	20	Cytoplasmic
sp|P06728|APOA4_MOUSE	Apolipoprotein A-IV OS=Mus musculus GN=Apoa4 PE=2 SV=2	19	Secreted
sp|P01029|CO4B_MOUSE	Complement C4-B OS=Mus musculus GN=C4b PE=1 SV=2	19	Secreted
sp|P12710|FABPL_MOUSE	Fatty acid-binding protein, liver OS=Mus musculus GN=Fabp1 PE=1 SV=2	18	Cytoplasmic
sp|P05784|K1C18_MOUSE	Keratin, type I cytoskeletal 18 OS=Mus musculus GN=Krt18 PE=1 SV=5	18	Cytoplasmic
sp|Q8BWT1|THIM_MOUSE	3-ketoacyl-CoA thiolase, mitochondrial OS=Mus musculus GN=Acaa2 PE=1 SV=2	17	Mito
sp|O08677|KNG1_MOUSE	Kininogen-1 OS=Mus musculus GN=Kng1 PE=1 SV=1	17	Secreted
sp|P68372|TBB2C_MOUSE	Tubulin beta-2C chain OS=Mus musculus GN=Tubb2c PE=1 SV=1	16	Cytoplasmic
sp|P11679|K2C8_MOUSE	Keratin, type II cytoskeletal 8 OS=Mus musculus GN=Krt8 PE=1 SV=4	16	Cytoplasmic
sp|Q8QZT1|THIL_MOUSE	Acetyl-CoA acetyltransferase, mitochondrial OS=Mus musculus GN=Acat1 PE=1 SV=1	16	Mito
sp|Q61703|ITIH2_MOUSE	Inter-alpha-trypsin inhibitor heavy chain H2 OS=Mus musculus GN=Itih2 PE=1 SV=1	16	Secreted
sp|P19157|GSTP1_MOUSE	Glutathione S-transferase P 1 OS=Mus musculus GN=Gstp1 PE=1 SV=2	16	Secreted
sp|Q91X72|HEMO_MOUSE	Hemopexin OS=Mus musculus GN=Hpx PE=1 SV=1	16	Secreted
sp|P99024|TBB5_MOUSE	Tubulin beta-5 chain OS=Mus musculus GN=Tubb5 PE=1 SV=1	15	Cytoplasmic
sp|Q922R8|PDIA6_MOUSE	Protein disulfide-isomerase A6 OS=Mus musculus GN=Pdia6 PE=1 SV=3	15	ER
sp|P25688|URIC_MOUSE	Uricase OS=Mus musculus GN=Uox PE=1 SV=2	15	Mito
sp|Q61425|HCDH_MOUSE	Hydroxyacyl-coenzyme A dehydrogenase, mitochondrial OS=Mus musculus GN=Hadh PE=1 SV=2	15	Mito
sp|Q63836|SBP2_MOUSE	Selenium-binding protein 2 OS=Mus musculus GN=Selenbp2 PE=1 SV=2	15	Secreted
sp|P22599|A1AT2_MOUSE	Alpha-1-antitrypsin 1-2 OS=Mus musculus GN=Serpina1b PE=1 SV=2	15	Secreted
sp|Q61646|HPT_MOUSE	Haptoglobin OS=Mus musculus GN=Hp PE=1 SV=1	15	Secreted

Shaded proteins listed under 'Location' are reported to be secreted.

Table S2. Proteins identified in the conditioned medium that do ('Secreted Proteins') and not harbour a N-terminal signal sequence 'Not Secreted'.

Please refer to the accompanying Table S2 (Excel spreadsheet).

Table S3. Transcriptomics data.

Please refer to the accompanying Table S3 (Excel spreadsheet). Tab 1- All probe sets detected; Tab 2- Transcripts that correspond to a classically secreted protein; Tab 3- Transcripts that correspond to a classically secreted protein and are significantly different ($P<0.05$) between hepatocytes derived from Chow and HFD fed mice (marked in red: upregulated transcripts, marked in blue: downregulated transcripts).

Supplementary Figures

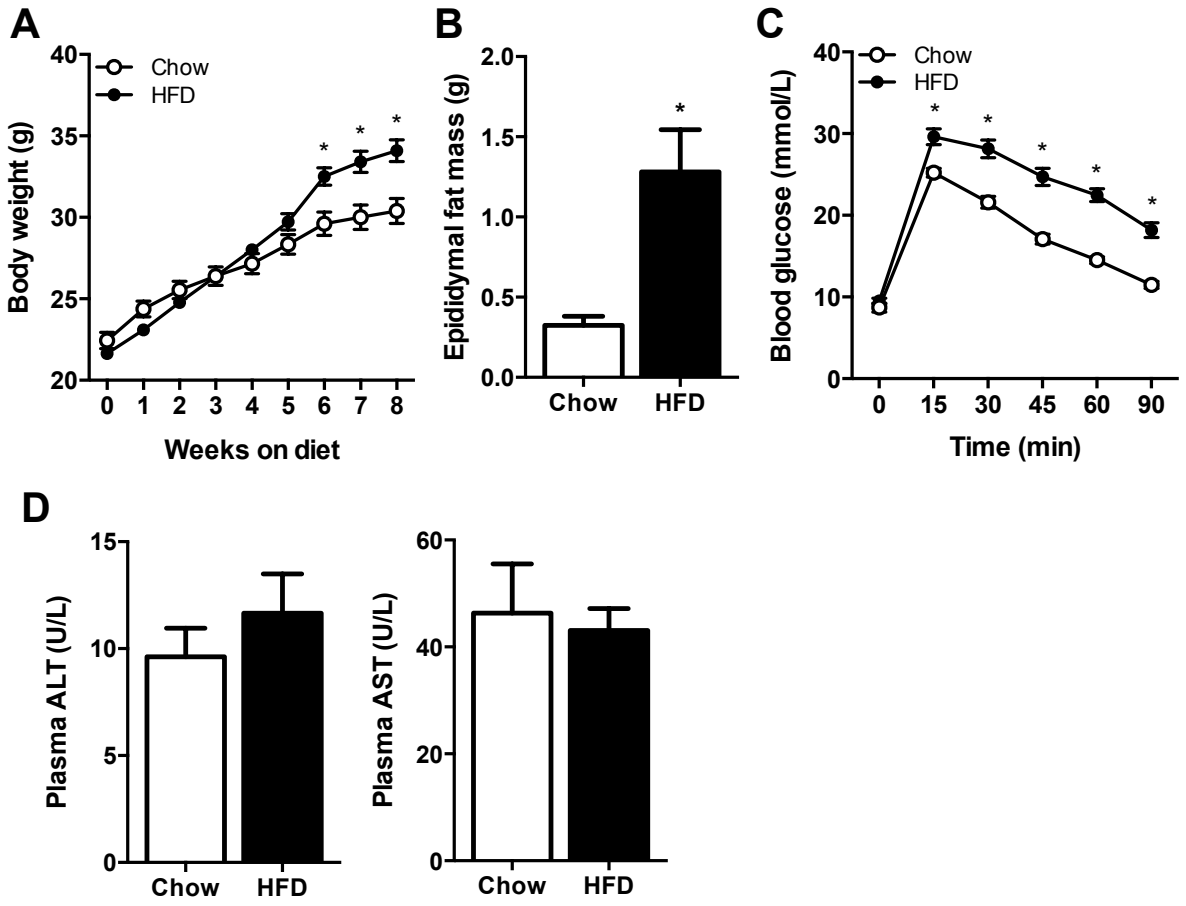

Figure S1. High-fat feeding causes hepatic steatosis, independent of inflammation.

C57Bl/6J mice were fed a chow or high-fat diet (HFD) for 6-8 weeks. **(A)** Body mass. **(B)** Epididymal fat mass. **(C)** Blood glucose responses to intraperitoneal glucose (2 g/kg) administration. **(D)** Liver damage markers plasma alanine aminotransferase (ALT) and aspartate aminotransferase (AST). (n=7-12 per group). *P<0.05 vs. Chow.

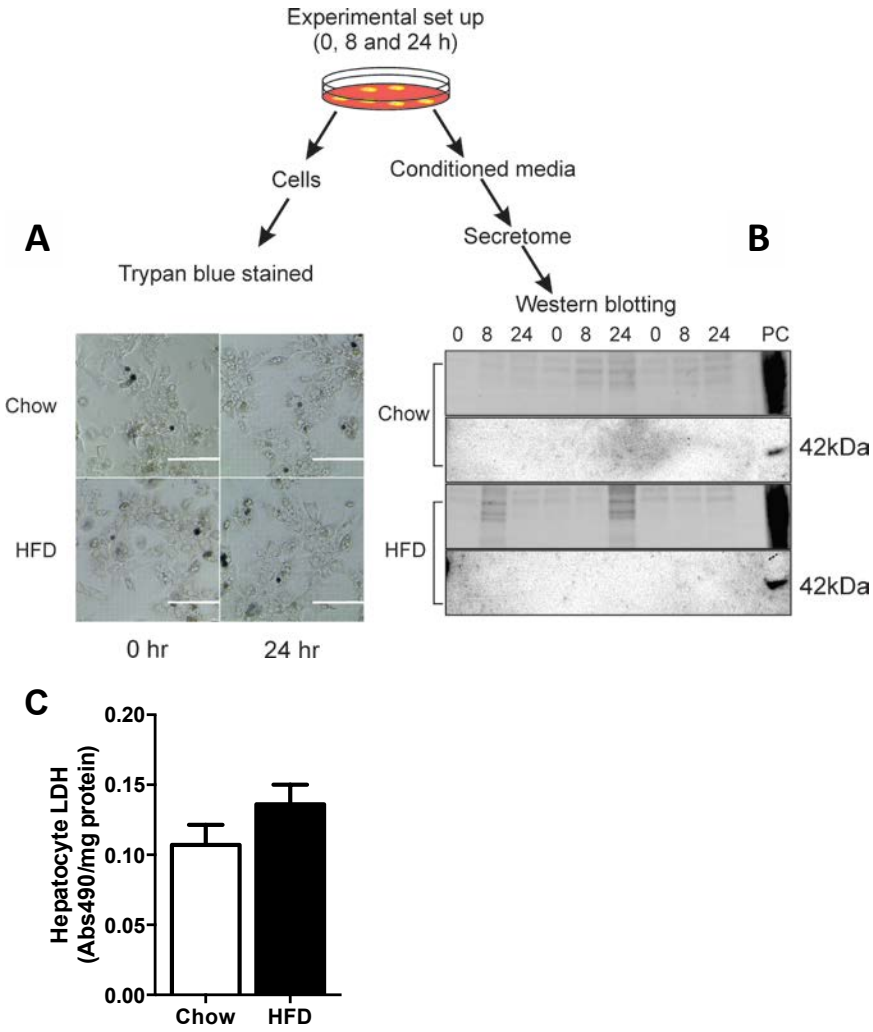

Figure S2. No evidence of significant cell death in the isolated hepatocyte culture.

(A) Hepatocytes isolated from mice fed a Chow or high-fat diets (HFD) were stained for trypan blue (indicating cell death) before and 24 h after the addition of the collection medium. Cell death was not different between 0 and 24 h or between treatment conditions. Scale bar = 200 μm. Images represent n=3 independent experiments. **(B)** No evidence of cytoskeletal actins in the culture medium. Hepatocytes isolated from mice fed a Chow or high-fat diet (HFD) were plated and once adherent, collection medium was added. The collection medium was removed after 0, 8 and 24 h and subjected to SDS-PAGE and immunodetection of β-actin. Top panel represents post-transfer image demonstrating total protein loading, bottom panel immunoblot against β-actin (5 min exposure). n=3 independent donor mice for Chow and HFD. PC- positive control, hepatocyte lysate. **(C)** Lactate dehydrogenase in the cell culture medium 24 h after plating. n=8 independent donor mice.

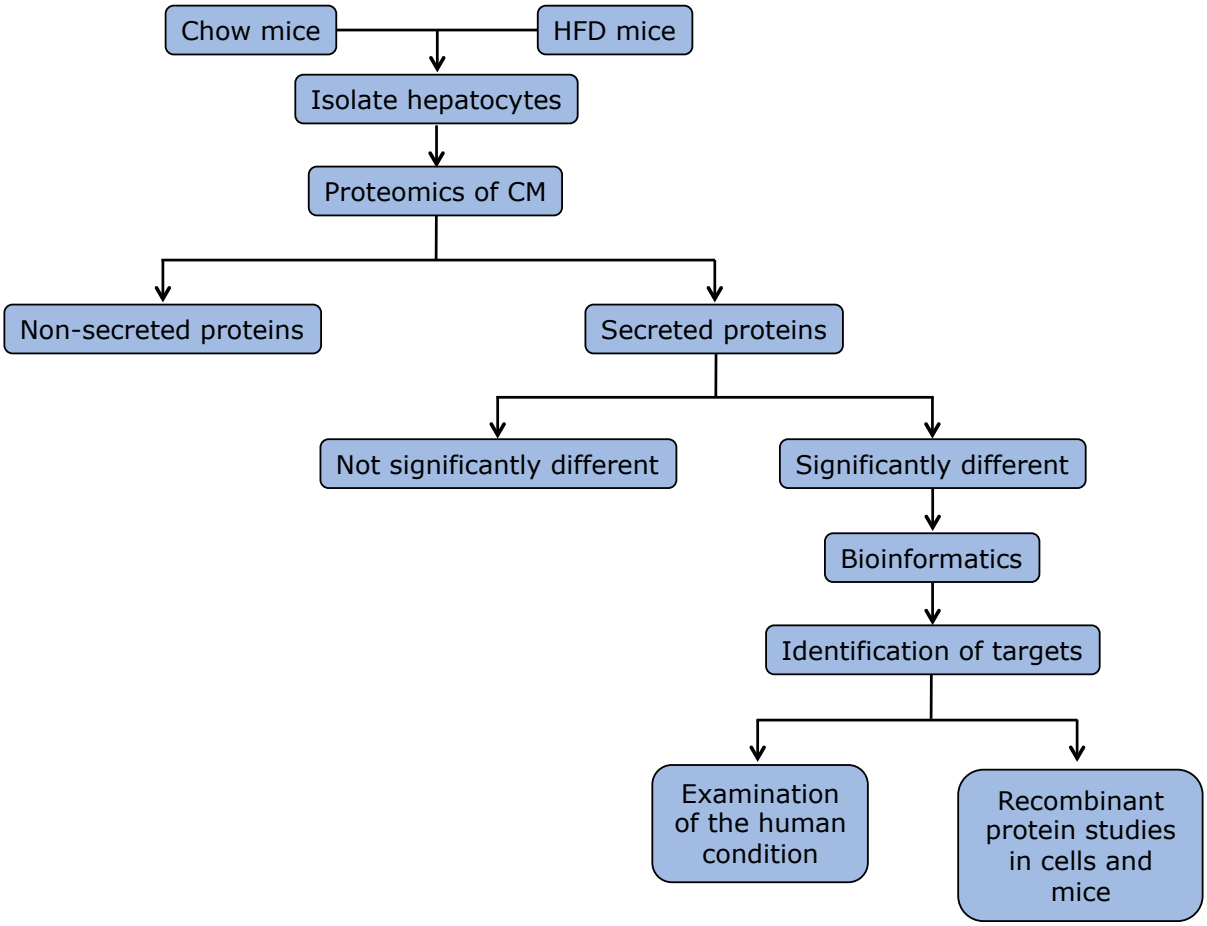

Figure S3. Workflow of the experiments.

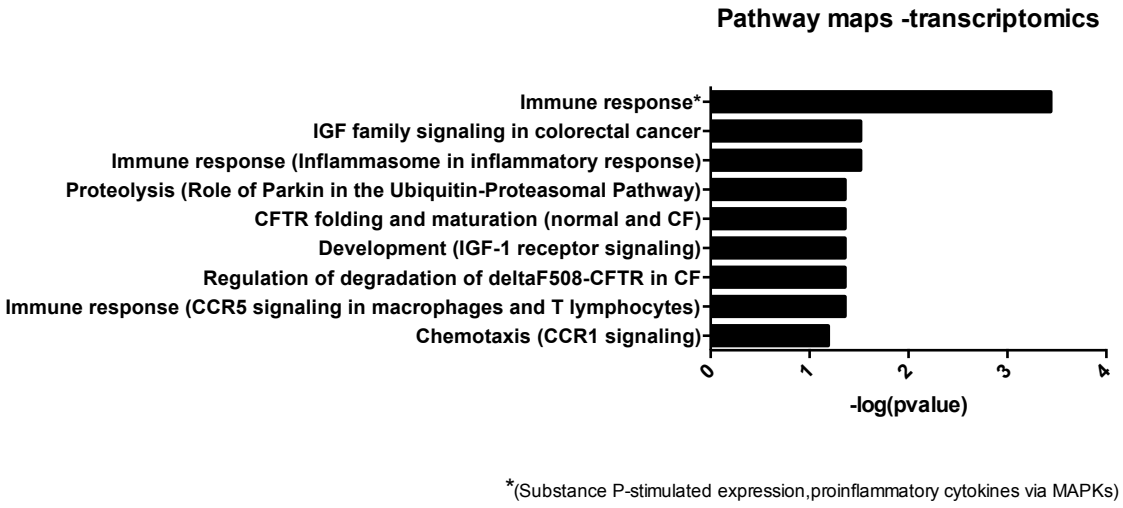

Figure S4. Enrichment analysis. Genes encoding secreted proteins that showed significant differences in expression between hepatocytes from mice a chow or HFD. Analysis was performed in comparison to a list of 'secreted proteins' that was generated using the 533 genes on the gene chip that are predicted to translate to secreted proteins.

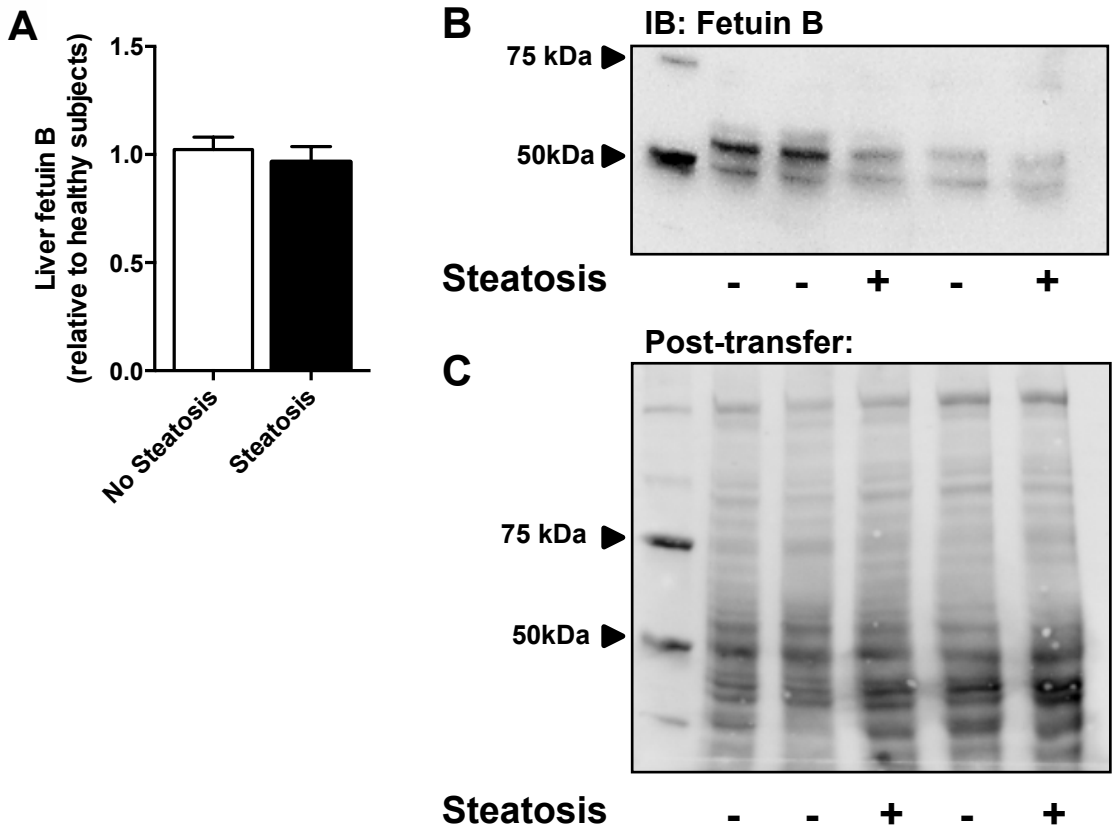

Figure S5. Fetuin B protein in human liver. **(A)** Fetuin B protein content in the livers of obese humans without (No Steatosis, n=14) or with liver steatosis (Steatosis, n=11). Fetuin B normalized to total protein loading for respective samples. **(B)** Representative immunoblot. (C) Protein loading for corresponding immunoblot.

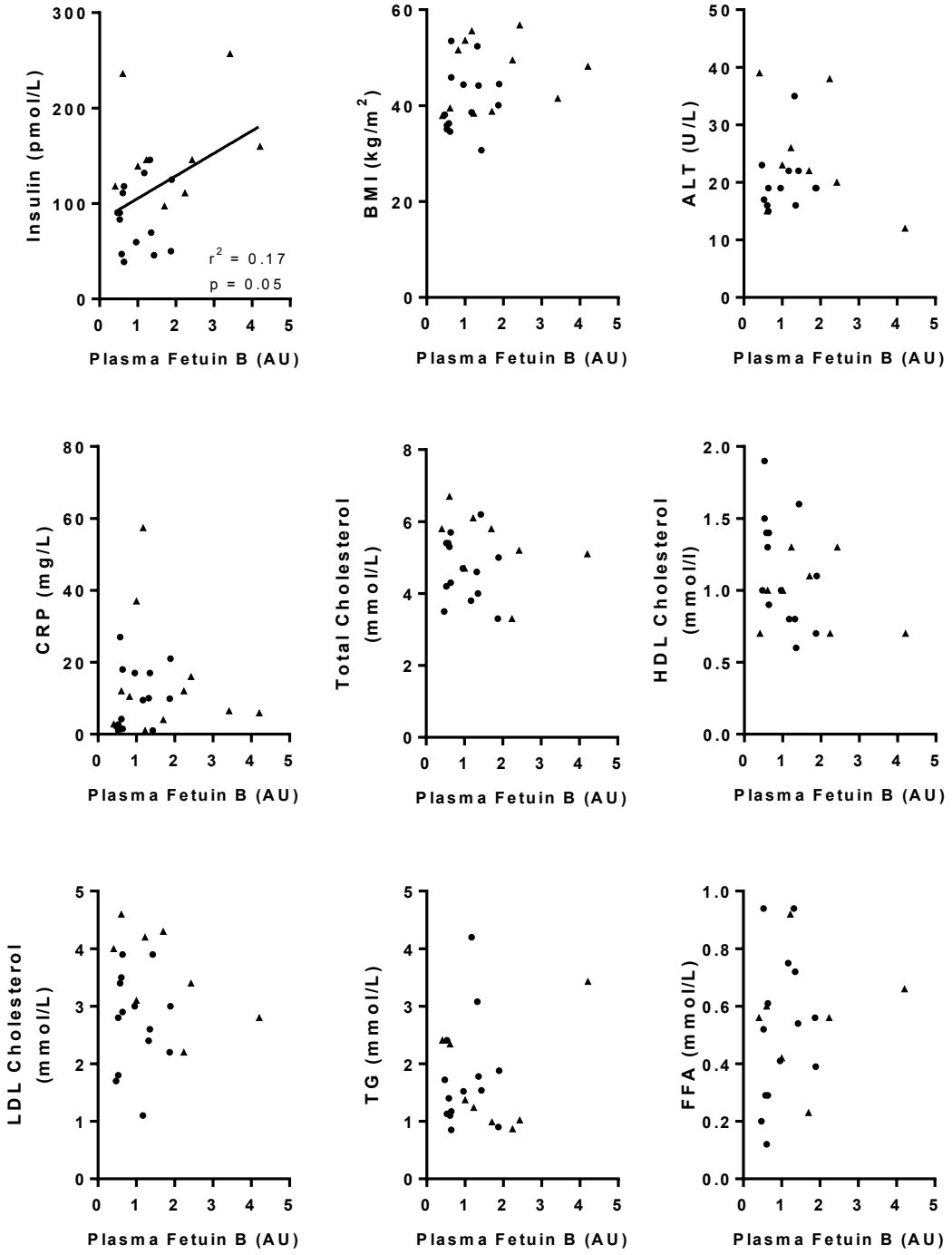

Figure S6. Relationship between plasma fetuin B and metabolic parameters. Closed circles, patients with no steatosis; closed triangles, patients with steatosis. N=23 for Fetuin B vs. BMI. N=21 for Fetuin B vs. insulin. N=20 for Fetuin B vs. ALT, CRP, total cholesterol, HDL cholesterol, LDL cholesterol, TG and FFA.

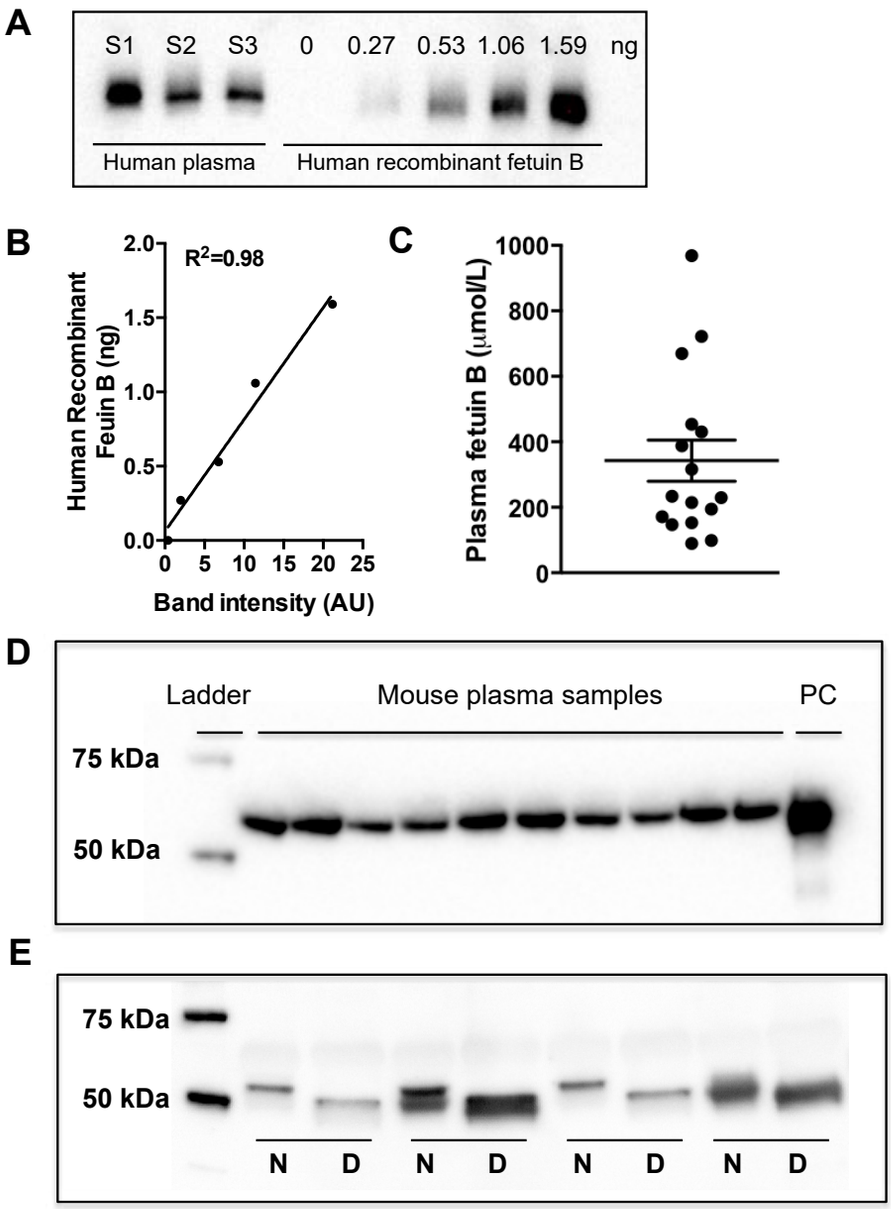

Figure S7. Fetuin B concentration in human plasma. (A) Immunoblot showing recombinant fetuin B and human plasma. **(B)** Standard curve demonstrating the relationship between recombinant human fetuin B and densitometry as assessed by immunoblot. **(C)** Fetuin B levels in human plasma, n=16. **(D)** Demonstration that the fetuin B antibody detects a single immunoreactive protein of the correct molecular mass in plasma (PC= human recombinant fetuin B). **(E)** Demonstration that the detect fetuin B is glycosylated. N = native protein, D = deglycoslyated protein in human plasma.

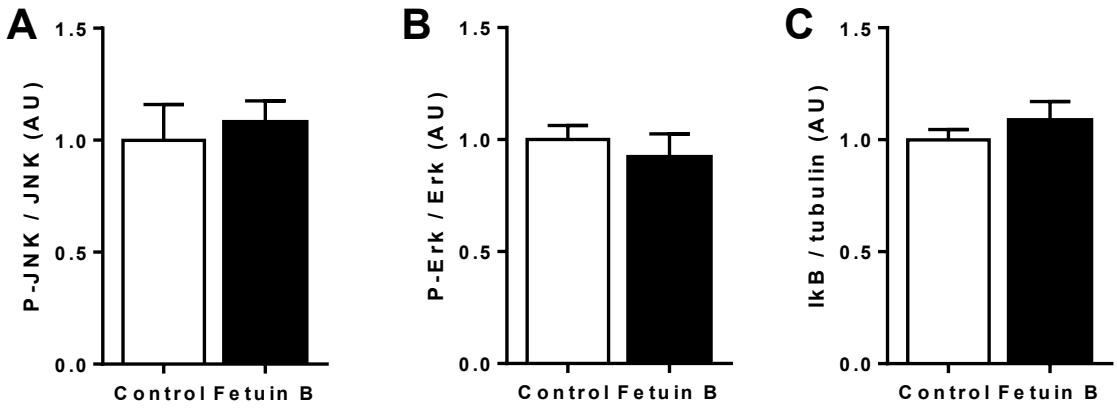

Figure S8. Fetuin B had no effect on pro-inflammatory signalling in myotubes as measured by phosphorylation of **(A)** JNK, **(B)** Erk, and expression of **(C)** IkBα. (n=3 per condition from 1 experiment).

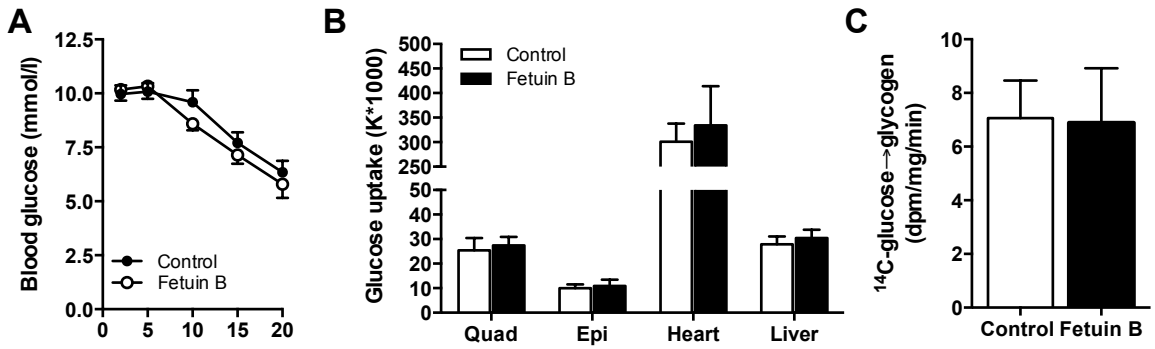

Figure S9: Fetuin B had no effect on whole-body or tissue-specific insulin action. Fetuin B was administered i.p 2 h prior to an intravenous insulin tolerance test. **(A)** blood glucose disposal whole-body insulin action, **(B)** tissue-specific insulin action, **(C)** glycogen storage.

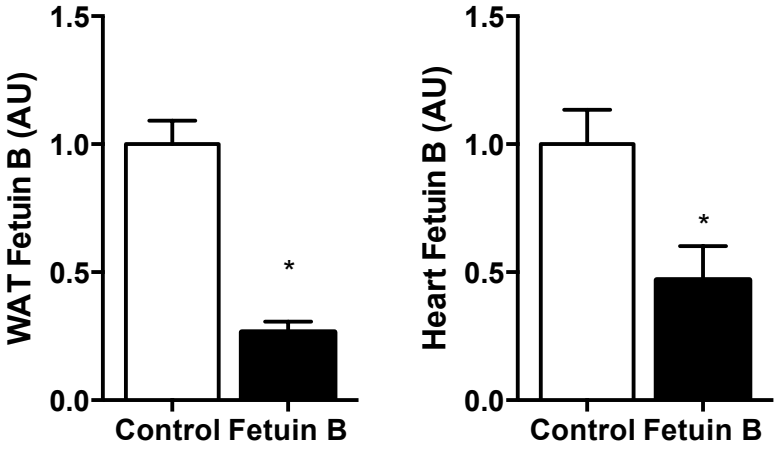

Figure S10: Fetuin B shRNA decreased fetuin B expression in white adipose tissue and heart compared with control (scramble shRNA). (n=10 Control, n=6 fetuin B shRNA).

*P<0.05 vs control.

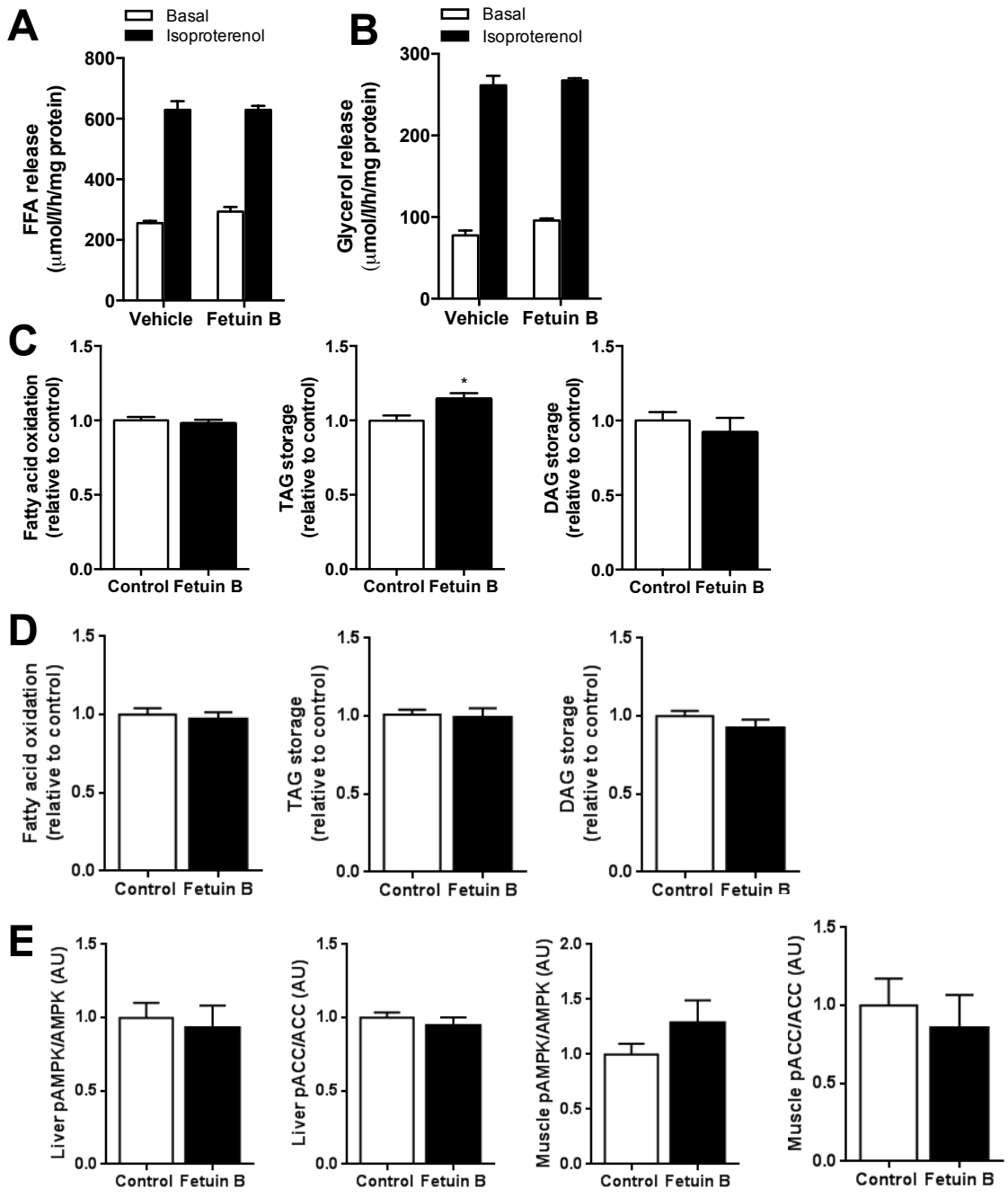

Figure S11: Fetuin B does not impact several regulators of glucose effectiveness or insulin action. (A-B) Adipocyte lipolysis determined by FFA release and glycerol release into the culture medium. (n=4 per condition from 1 experiment). **(C)** Fatty acid metabolism in L6 GLUT4myc myotubes. (n=3 biological replicates, each performed with 4 technical replicates). *P<0.05 vs control. **(D)** Fatty acid metabolism in primary hepatocytes. (n=3 biological replicates, each performed with 4 technical replicates). **(E)** AMPK signalling in muscle and liver on mice 3 h after fetuin B injection i.p. (n=11 per group).

Supplementary Experimental Procedures

Human experiments

Twenty-five obese subjects undergoing bariatric surgery at the Maastricht University Medical Centre participated in this study (see Table 1 for subject characteristics). No subject presented with autoimmune diseases, hepatitis, or self-reported excessive alcohol intake (20 g/day). The institutional medical ethical committee of Maastricht University approved the study, and all subjects provided written informed consent before participation. A fasted plasma sample was obtained before surgery from each subject and a liver biopsy was taken during surgery to assess the presence of liver steatosis according to the Brunt classification (Brunt et al., 1999). Subjects were divided into two groups. The healthy group (n=14) comprised patients with <5% steatotic hepatocytes (score 0). The steatotic group (n=11) comprised patients with >5% steatotic hepatocytes (score 1-3) without significant inflammation as observed after H&E staining (i.e. no intra-acinar inflammatory foci per 20 fields with a 20 ocular and no portal tract inflammation).

A second study included 28 age-matched males who were lean insulin-sensitive (n=9), obese insulin-sensitive (n=5) and obese with type 2 diabetes (n=14). Some of these samples were used in a previous study (Boon et al., 2013). Type 2 diabetes was defined as a fasting plasma glucose > 7 mmol/L and or plasma glucose > 11.1 mmol/L 2 hours after a 75g oral glucose load. None of the participants received insulin, oral hypoglycemic or statins. Venous blood samples were obtained from an antecubital vein after an overnight fast, immediately centrifuged and the plasma frozen at -80^{o}C until analysis. The study was approved by the Alfred Hospital human research ethics committee, was conducted in accordance with the declaration of Helsinki, and all participants provided written informed consent before participation in the study.

Animal care and maintenance

The Monash University School of Biomedical Science Animal Ethics Committee approved surgical and experimental procedures. Male C57BL/6 mice aged 8 weeks were purchased from Monash Animal Services. All mice were bred and housed under controlled temperature (22°C) and lighting (12:12 h light-dark cycle), and were fed either a chow (Specialty Feeds Irradiated Rat and Mouse Pellets; 19.6% energy from protein, 4.6% fat, 4.8% crude fibre, 14.3 MJ/Kg energy) or high fat diet (Specialty Feeds SF03-002; 19.5% protein, 36% fat, 4.7% crude fibre, 22.8 MJ/kg energy) *ad libitum* for 6 weeks.

Glucose tolerance test

A glucose tolerance test in mice was performed at 14 weeks. Mice were fasted for 4 h and injected with 2 g/kg glucose (50% dextrose solution) in the intraperitoneal cavity. Blood glucose and lactate levels were analysed via tail bleeds before and at 15, 30, 45, 60 and 90 min post injection. For the fetuin B experiments, mice were injected with either saline or human recombinant fetuin B (1 μg/g body mass) (Life Research) 2 h prior to the glucose tolerance test. For insulin signalling experiments, mice were anesthetized (3% isoflurane) 15 min after glucose administration and livers and skeletal muscle freeze-clamped *in situ* for later analysis. In separate experiments, mice were fed a HFD for 6 weeks. After week 1, an adenoassociated virus serotype 8 (AAV8) driven by a CMV promoter ($1x10^{12}$gc), containing an shRNA sequence specific for murine fetuin B (Vector Biolabs, shADV-259329) was injected via the tail vein. Control mice were injected with the same vector containing LacZ.

Hepatocyte isolation

Mice were anaesthetized with 3% isofluorane (Isorrane Inhalation Anaesthetic, Baxter) and a 24 gauge catheter was inserted into the hepatic portal vein. The liver was perfused with 50 ml of Hanks Buffered Salt Solution (HBSS) maintained at 37°C using a peristaltic pump

(Pharmacia Biotech P-1). Thereafter, the liver was perfused with 50 ml of collagenase buffer containing Liberase TM Research Grade (50 μg/ml) (Roche). The inferior vena cava was severed upon commencing the perfusion to allow drainage of the perfusate. The liver was dissected upon completion of the perfusion, minced with scissors, filtered through a 70 μm filter and after three washes in Hanks buffer, the hepatocytes were resuspended in filtered M199 medium as described below. The purity of hepatocytes was established in preliminary experiments by fluorescence-activated cell sorting.

Cell culture and in vitro experimental design. Isolated primary hepatocytes were plated into tissue culture dishes in filtered M199 medium supplemented with 10% FBS, 1% penicillin-streptomycin (Gibco), 100 nM insulin (Sigma), 400 nM dexamethasone (Sigma) and 1.5 nM EGF (BD Biosciences). After four hours, the media was replaced with the same medium and supplements and 10 nM insulin. The culture medium was changed after 24 h and subsequent experiments were conducted 24-48 h later.

Immunofluorescence staining of hepatocytes

Cultured hepatocytes were fixed with 10% NBF for 10 minutes followed by 90 seconds permeabilisation with 0.1% Triton X in 10% NHS prior to washing. Non-specific antibody binding was minimized by blocking samples using Mouse On Mouse (MOM) blocking reagent (Vector) and followed by 1% BSA for 1 hour at room temperature. Anti-CD45 (BD Biosciences), anti-CD31 (BD Pharmingen) and anti-F4/80 (supplied by collaborator) were applied and incubated overnight at 4°C. Samples were washed and followed by incubation with the appropriate secondary antibody. DNA was visualized using 1 μg/ml 4',6-diamidino-2-phenylindole (DAPI). Images were taken with a Leica TSC SP8 confocal invert microscope in the Monash University Microimaging Facility.

Trypan blue staining of adherent cells

Culture medium was removed from hepatocytes and 0.2% trypan blue solution (Life technologies) diluted with 1X PBS was added and incubated for 1 minute. Trypan blue solution was removed and replaced with 1X PBS prior bright field imaging using EVOS® XL imaging system (Life Technologies).

Immunoblot analysis of secreted proteins

Reducing sample buffer was added to conditioned medium and boiled at 95°C for 7 minutes before separation using 10% Mini-PROTEAN® TGX™ Gel. Proteins were transferred onto PVDF membrane, blocked with 5% skim milk in 1X PBS then probed with anti-actin (Abcam) and appropriate secondary antibody. Membranes were then incubated with Clarity™ western ECL blotting substrate and immune-reactive bands were visualised using ChemiDoc™ Imaging Systems (Biorad).

Lipid staining of culture hepatocytes

Cultured hepatocytes were rinsed once with 1X PBS and lipid droplets were stained using 2 µg/ml of Nile red diluted with 150 mM NaCl for 10 minutes in the dark. Hepatocytes were then fixed with 10% neutral buffered formalin (NBF) and washed with 1X PBS prior mounting with fluorescence mounting medium (Dako). Images were taken using Leica TCS SP8 confocal invert microscope in the Monash University Microimaging Facility.

Flow cytometry

Primary hepatocytes were stained with Alexa-fluor 700 anti-CD45, PE-Cy7 anti-F4/80 (Biolegend) and unconjugated anti-CD31 (supplied by collaborator) for 30 minutes on ice. After washes with 1X PBS, 1mM EDTA, secondary antibody were applied and incubated for 30 minutes on ice. Cells were washed and propidium iodide was used to distinguish between

live and dead cells. Cells were analysed using LSR II (BD Biosciences) and data analysis was completed using Flowjo cytometric analysis program (version 10).

Biochemical measures. Hepatocyte lipids were extracted in chloroform:methanol (2:1) and triacylglycerol content was determined by enzymatic colorimetric assay (GPO-PAP reagent, Roche Diagnostics). Alanine aminotransferase (ALT) and aspartate transaminase (AST) were determined using commercial kits (Thermo Scientific, Melbourne, Australia). Lactate dehydrogenase activity was assessed by LDH cytotoxicity Kit (Pierce)**.**

Validation of immunological detection of Fetuin B in human tissue and plasma samples

Plasma was diluted 1/80 in water and mixed with equal amounts of 2 x Laemmli buffer (Biorad). Samples were boiled for 5 minutes at 95°C, and 20 µl of sample was loaded into the wells for SDS-PAGE. This corresponds to 0.125 µl of plasma. Human liver was homogenized in RIPA lysis buffer (65mM Tris, 150mM NaCl, 1% NP40, 0.5% sodium deoxycholate, 0.1% SDS, 10% glycerol, pH 7.4) containing 1 mM DTT, protease inhibitors (cOmplete 195 Protease Inhibitor Cocktail; Roche Diagnostics, Castle Hill, NSW, Australia (1 tablet per 50 ml of lysis buffer, as per manufacturer's recommendations)) and phosphatase inhibitors (PhosSTOP Phosphatase Inhibitor Cocktail; Roche Diagnostics (1 tablet per 10 ml of lysis buffer, as per manufacturer's recommendations)). After centrifugation, protein concentration was determined (Pierce BCA assay, Thermo Scientific, Rockford, IL); samples were solubilized in 2x laemmli buffer (Biorad) and boiled for 5 minutes at 95°C. Equal amounts of protein (30 µg) were loaded into 7.5% Criterion precast stain-free gels (Bio-Rad Laboratories, NSW, Australia), subjected to SDS-PAGE and transferred to PVDF membranes (Trans-Blot® Turbo™ Transfer System, Bio-Rad Laboratories, NSW, Australia). For all immunoblots, equal numbers of subjects with and without steatosis were loaded on the gels. Membranes were blocked with 5% milk in TBST, washed 3 times for 5 min in TBST, and

probed with a rabbit polyclonal antibody raised against Fetuin B (Genetex, GTX112260) (dilution 1/1000 in TBST + 5% BSA) for 1h at room temperature on a rocker. After washing 3 times for 5 min in TBST, the membranes were probed with the appropriate secondary antibody (Anti-rabbit ECL IgG, NA934OV, GE Healthcare) (dilution 1/2000 in 5% milk in TBST), and bands were detected with enhanced chemiluminescence as per the manufacturer instructions (Clarity™ Western ECL Substrate, Bio-Rad Laboratories, NSW, Australia) using the ChemiDoc™ MP System (Bio-Rad Laboratories, NSW, Australia), and quantified by densitometry (ImageLab, Version 4.1, Bio-Rad, NSW, Australia). The immunoreactive signal was normalized to the density of the total protein loading for each sample, which was obtained by visualization of the stain-free blot image and quantified using ImageLab.

We performed experiments to confirm that the antibody was detecting secreted fetuin B.

(a) Demonstration of correct molecular mass. This experiment shows that the detected protein migrates at the same molecular mass as recombinant human fetuin B (Fig. S7D)

(b) Deglycosylation experiment. To remove carbohydrate residues from fetuin B, plasma was treated with PNGaseF (Biolabs) as per the manufacturer instructions. In short 0.125 µl of plasma was diluted in 9 µl of water (1/80 dilution), combined with 1 µl Glycoprotein Denaturing buffer, and denatured by heating reaction at 100 °C for 10 minutes. After denaturing, the total reaction volume was increased to 20 µl by adding 2 µl of 10x G7 Reaction Buffer, 2 µl NP40, 5 µl water and 1 µl PNGaseF, and incubated at 37°C for 1 h. Samples were diluted with 2x Laemmle buffer, and the sample was loaded on a 7.5% Criterion precast stain-free gel for immunoblotting as described above. This study demonstrates that we are detecting a glycosylated protein (Fig. S7E).

(c) Fetuin B concentration in plasma. To determine the concentration of fetuin B in human plasma, 0.125 µl of human plasma and human recombinant fetuin B (0, 0.27, 0.53, 1.06, 1.59 ng; Sino Biological) were diluted in water to a total volume of 10 µl. Samples were combined with 10 µl of 2x Laemmle buffer, boiled at 95°C for 5 minutes, and loaded on a 7.5%

Criterion precast stain-free gel for immunoblotting as described above. The plasma fetuin B concentration was quantified by determining the relationship between the recombinant human fetuin B and densitometry. The standard curve is shown in Fig S7B.

Immunoblotting of cells and tissues. Cells were washed in ice-cold PBS and homogenized in RIPA lysis buffer as described above. Equal amounts of protein (30 µg) were loaded into 7.5% Criterion precast stain-free gels (Bio-Rad), subjected to SDS-PAGE and transferred to PVDF membranes (Bio-Rad). For all immunoblots, equal numbers of control and fetuin B samples were loaded on the gels. Membranes were blocked with 5% milk in TBST, washed in TBST, and probed with the primary antibody, at 4°C overnight on a rocker. Primary antibodies (dilution 1/1000 in TBST + 5% BSA) for anti-pAkt ser 473 (#9271), anti-Akt (#9272), anti-pERK Thr202/Tyr204 (#9101), anti-ERK (#4695), anti-pJNK Thr183/Tyr185 (#4668), anti-JNK (#9252), anti-IkB (#9242), anti-Tubulin (#2148), anti-pACC Ser79 (#3661), anti-ACC (#3676), anti- pAMPKα Thr172 (#2531), anti-AMPKα (#2532), anti-IRS1 (#3194), anti-pP70S6K Thr389 (#9205), anti-P70S6K (#9202), anti-pIR ϒ1361 (#3023), anti-IR (#9202) and anti-pGSKα/β S21/9 (#9331) were purchased from Cell Signaling (Danvers, MA). Anti-pIRS1 pϒ612 (#44-816G) was purchased from Invitrogen. Blots were probed with the appropriate secondary antibody (1/4000 in 5% milk in TBST) and after incubation specific protein bands were visualized with enhanced chemiluminescence using the ChemiDoc™ MP System, and quantified by densitometry as described above. The immunoreactive signal was normalized to the density of the total protein loading for each sample, which was obtained by visualization of the stain-free blot image.

qRT-PCR

Cells were lysed in Qiazol and total RNA was extracted. Reverse transcription of 1 µg mRNA was performed (iScript cDNA Synthesis Kit, Bio-Rad Laboratories, Hercules, CA),

and gene products were determined by quantitative real-time PCR (Realplex Mastercycler, Eppendorf) using the TaqMan Universal PCR Master Mix and TaqMan Gene Expression Assays for *Glc-6-p* and *Pepck*. The relative quantification was calculated using the ΔΔCt method, using 18S rRNA as the housekeeping gene and values were normalized to the control condition.

Conditioned media collection.

Hepatocytes were washed with PBS then incubated in EX-CELL® 325 Protein-Free CHO Serum-Free Medium (SAFC Biosciences). Conditioned media (CM) was collected after 24 h, centrifuged at 300 x g and the media collected and stored at -80°C. Cells were scraped for the assessment of total protein content (BCA Protein Reagent, Pierce) and for transcriptomic analysis.

Conditioned medium experiments

Primary bone marrow-derived macrophages (BMDM) and L6 GLUT4myc myotubes were cultured as described previously (Boon et al., 2013; Lancaster et al., 2014). Cells were pre-treated with CM from Chow or HFD hepatocytes for 16 h. Macrophages were treated with lipopolysaccharide **(**LPS, Invivogen) for 30 min then collected for immunoblot analyses. Fatty acid metabolism was assessed in myotubes by radiometric techniques as described (Turpin et al., 2010). Briefly, [1-^{14}C]oleic acid (0.25uCi/ml; Perkin Elmer) and 0.5 mM unlabeled oleic acid were conjugated to 2% BSA (w:v) and oxidation and storage in intracellular pools were determined. 2-Deoxy-D-glucose (2DG) uptake was determine in myotubes by adding 2-Deoxy-D-[1,^{3}H] glucose (1 mM, 0.5 μCi /ml) (Perkin Elmer) and D-[1-^{14}C]mannitol (8 mM, 0.2 μCi /ml) (GE Healthcare /Quantum) to Krebs buffer containing 0.1% BSA. Cells were treated with PBS (basal) or 10 nM insulin and 2DG uptake was

measured over 20 min. Cells were washed three times in ice-cold PBS and lysed. 2DG was measured using liquid scintillation counting, and values were normalised to protein content.

iTRAQ sample preparation and data acquisition. 2.5 mL of each conditioned media from mouse hepatocytes were buffer exchanged into 0.5 M triethylammonium bicarbonate, 0.02% (w/v) SDS by ultrafiltration at 3000 *g* using a Vivaspin 5000 MWCO device (Sartorius, Bohemia, NY). Proteins were reduced with TCEP, alkylated with MMTS, digested with trypsin and labelled with iTRAQ 8-plex reagents following the manufacturer's instructions as we previously described (Song et al., 2008). The iTRAQ labeled samples (4 HFD, 4 vehicle control) were combined in equal ratios and fractionated by strong cation exchange chromatography to yield 12 fractions. Each fraction was dried, re-suspended in 0.1% trifluoroacetic acid, 2% acetonitrile and loaded onto a reversed-phase Captrap (Michrom Bioresources, CA). Following desalting, the trap was switched in-line with a 150 µm x 10 cm, C18 3µm 300Å ProteCol column (SGE, Ringwood, Vic) and analysed by nanoLC ESI MS/MS using a 120 min gradient with a Top 10 data dependent acquisition strategy with a 5600 TripleTOF mass spectrometer (AB Sciex, Redwood City, CA).

Proteomic data analysis. ProteinPilot v4.0 (AB Sciex) was used for iTRAQ data processing. The SwissProt 2010 *Mus musculus* database containing 32614 entries (fwd + rev) was searched. In the ProteinPilot parameter settings, the thorough search mode was used, the precursor ion mass tolerance was 0.05 Da, the product ion mass tolerance was 0.1 Da, Unused Prot Score was >1.3 (95% confidence, corresponding to 0.3% protein FDR) and bias correction was enabled. The protein iTRAQ ratios are the geometric means of corresponding peptide iTRAQ ratios, which require a minimum of 2 peptide spectrum matches. Differentially expressed proteins were determined by an unpaired two sample T-test ($p<0.05$).

Bioinformatics.

Cross-referencing of genes and protein accessions was performed using PICR (Wein et al., 2012) and UniProt cross-references. A secreted protein was defined as either presence of a signal peptide with absence of a transmembrane domain or annotation in UniProt by keyword (Secreted), GeneOntology cellular compartment (GO:0005576 or GO:0005615) or curation of subcellular comments.

Transcriptomics

The quality and quantity of mouse amplified RNA was ascertained on the Agilent Bioanalyser 2100 using the NanoChip protocol. A total of 750 ngs of amplified RNA was then prepared for hybridisation to the *Ilumina Mouse-ref8 Expression Beadchip* by preparing a probe cocktail (cRNA @ 0.05ug/ul) that includes GEX-HYB Hybridisation Buffer (supplied with the beadchip). A total hybridisation volume of 15ul was prepared for each sample and 15ul loaded into a single array on the *Ilumina Mouse-ref8 Expression Beadchip.* A total of 8 different labelled samples can be loaded into 8 individual arrays per beadchip. The chip was then hybridised at 58^{o}C for 16 hours in an oven with a rocking platform. After hybridisation, the chip was washed using the appropriate protocols as outlined in the Illumina manual. Upon completion of the washing, the chips were then coupled with Cy3 and scanned in the Illumina iScan Reader. The scanner operating software, GenomeStudio, converts the signal on the array into a TXT file for analysis. Genes with an expression difference of ≥ 1.20-fold with 95% confidence interval between the conditions were considered to be different.

Functional annotation of proteomic and transcriptomic data

The Metacore knowledge database and software suite (Thomson Reuters, Inc., New York, USA) 'enrichment analysis' function was used to identify biological processes (pathway

maps) over-represented by i) secreted proteins that differed in abundance and ii) genes encoding secreted proteins that differed in abundance / expression in the culture medium and hepatocytes of mice fed with chow or HFD. Enrichment analysis was performed against mouse proteins defined as secreted in the Uniprot data base for the proteomics data or, for transcriptomics, the 533 genes on the Illumina Mouse Ref 8 chip predicted to translate into secreted proteins were used. The biological processes are ranked based on the likelihood that the assembly of the proteins or genes within a given category occurred by random chance, which is displayed as a p-value.

Fetuin B cell experiments

L6 GLUT4myc myotubes were treated with fetuin B 24 h. For immunoblot analysis cells were treated with either PBS (basal) or 10 nM insulin before lysing. Fatty acid metabolism and insulin sensitivity was described as above. Fetuin B concentrations and incubation times are provided in figure legends.

Hyperinsulinemic-euglycemic clamps

Mice were catheterized 4 days before hyperinsulinemic, euglycemic clamp studies. Mice were anesthetized with isoflurane (1–2% in oxygen), and the right jugular vein was catheterized with a Silastic catheter (0.025-inch outer diameter). The catheter was exteriorized at the back of the neck, filled with sterile saline, and sealed with a stainless steel plug. Mice were fasted for 4 h prior to beginning the clamp. Mice were conscious but restrained for the duration of the procedure. Mice were injected IP with human recombinant fetuin B (1 μg/g body mass) (Life research) or heat-inactivated albumin 2 h prior to clamps. Blood glucose was equilibrated with a 90 min continuous infusion of [3-^{3}H]-glucose (0.05 μCi/min). Hyperinsulinemic-euglycemic clamp commenced with the increase of [3-^{3}H]-glucose tracer to 2 μCi/min and insulin infusion (4 mU/kg/min). Exogenous glucose (30%

w/v) was infused to maintain constant blood glucose levels. Tail blood samples were collected and blood glucose was measured every 5 min. At the conclusion of the clamp, mice were anaesthetized with an intravenous injection of sodium pentobarbitone (100 mg/kg iv) and tissues rapidly dissected and snap frozen in liquid nitrogen for further analysis.

Intravenous insulin tolerance test

The intravenous tolerance test was performed according to previously published work (Borg et al., 2014).

Statistical analysis

Statistical analysis was performed using unpaired one or two-way Student's t-tests, two-way analysis of variance (ANOVA) or repeated measures ANOVA where appropriate. Multiple comparisons were performed using a Bonferroni post hoc analysis when required. Statistical significance was set *a priori* at $P \leq 0.05$. Data are reported as means ± SEM.

Supplementary References

Boon, J., Hoy, A.J., Stark, R., Brown, R.D., Meex, R.C., Henstridge, D.C., Schenk, S., Meikle, P.J., Horowitz, J.F., Kingwell, B.A., et al. (2013). Ceramides Contained in LDL Are Elevated in Type 2 Diabetes and Promote Inflammation and Skeletal Muscle Insulin Resistance. Diabetes *62*, 401-410.

Borg, M.L., Lemus, M., Reichenbach, A., Selathurai, A., Oldfield, B.J., Andrews, Z.B., and Watt, M.J. (2014). Hypothalamic neurogenesis is not required for the improved insulin sensitivity following exercise training. Diabetes.

Brunt, E.M., Janney, C.G., Di Bisceglie, A.M., Neuschwander-Tetri, B.A., and Bacon, B.R. (1999). Nonalcoholic steatohepatitis: a proposal for grading and staging the histological lesions. Am J Gastroenterol *94*, 2467-2474.

Lancaster, G.I., Kraakman, M.J., Kammoun, H.L., Langley, K.G., Estevez, E., Banerjee, A., Grumont, R.J., Febbraio, M.A., and Gerondakis, S. (2014). The dual-specificity phosphatase 2 (DUSP2) does not regulate obesity-associated inflammation or insulin resistance in mice. PLoS One *9*, e111524.

Song, X., Bandow, J., Sherman, J., Baker, J.D., Brown, P.W., McDowell, M.T., and Molloy, M.P. (2008). iTRAQ experimental design for plasma biomarker discovery. J Proteome Res *7*, 2952-2958.

Turpin, S.M., Hoy, A.J., Brown, R.D., Garcia Rudaz, C., Honeyman, J., Matzaris, M., and Watt, M.J. (2010). Adipose triacylglycerol lipase is a major regulator of hepatic lipid metabolism but not insulin sensitivity in mice. Diabetologia.

Wein, S.P., Cote, R.G., Dumousseau, M., Reisinger, F., Hermjakob, H., and Vizcaino, J.A. (2012). Improvements in the Protein Identifier Cross-Reference service. Nucleic Acids Res *40*, W276-280.

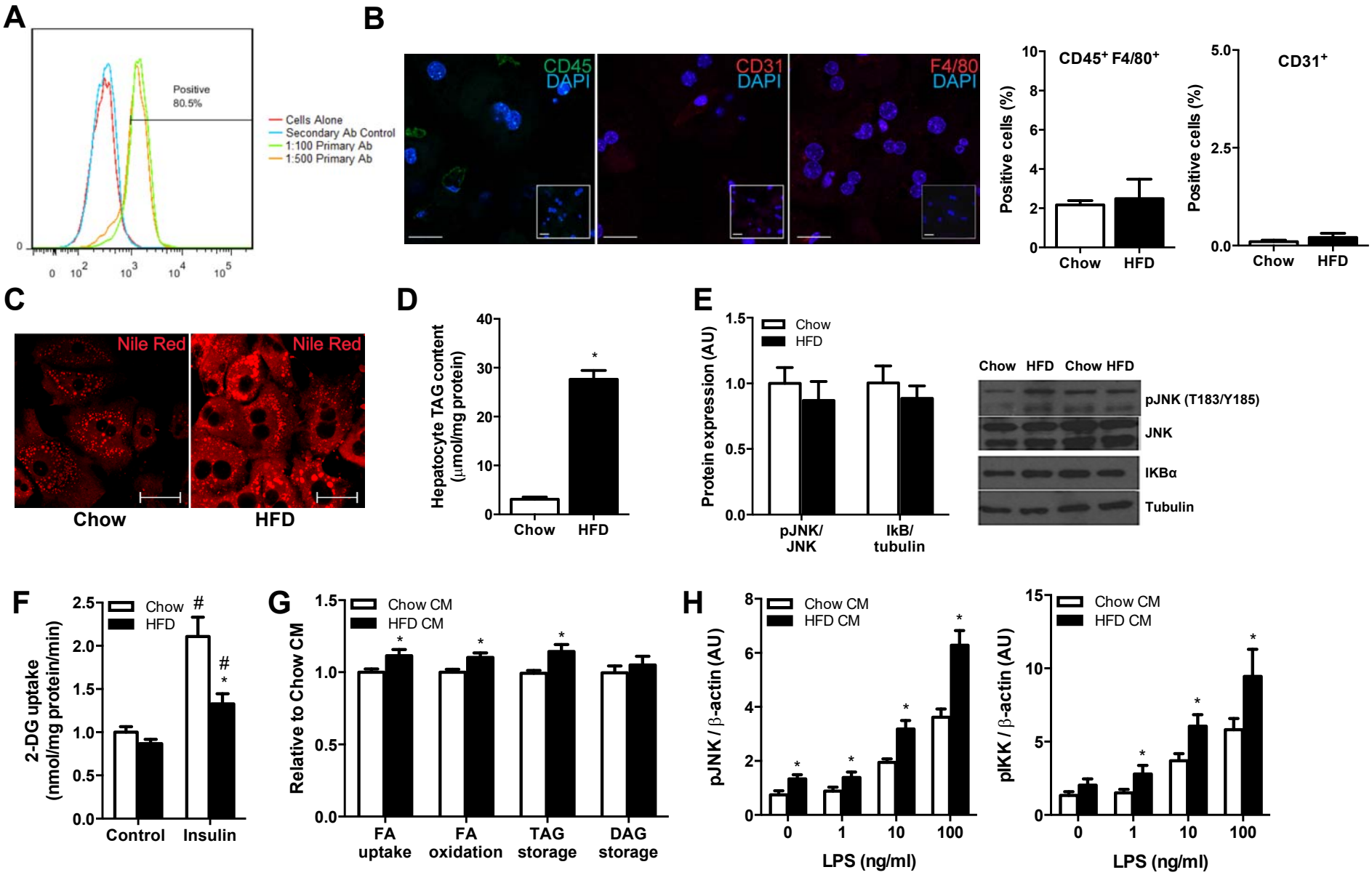
A
Positive
80.5%
Cells Alone
Secondary Ab Control
1:100 Primary Ab
1:500 Primary Ab
B
CD45
DAPI
CD31
DAPI
F4/80
DAPI
CD45+ F4/80+
Positive cells (%)
Chow
HFD
CD31+
Positive cells (%)
Chow
HFD
C
Nile Red
Nile Red
Chow
HFD
D
Hepatocyte TAG content
(μmol/mg protein)
Chow
HFD
E
Protein expression (AU)
Chow
HFD
pJNK/
JNK
IkB/
tubulin
Chow HFD Chow HFD
pJNK (T183/Y185)
JNK
IKBα
Tubulin
F
2-DG uptake
(nmol/mg protein/min)
Chow
HFD
Control
Insulin
G
Relative to Chow CM
Chow CM
HFD CM
FA
uptake
FA
oxidation
TAG
storage
DAG
storage
H
pJNK / β-actin (AU)
Chow CM
HFD CM
LPS (ng/ml)
pIKK / β-actin (AU)
Chow CM
HFD CM
LPS (ng/ml)

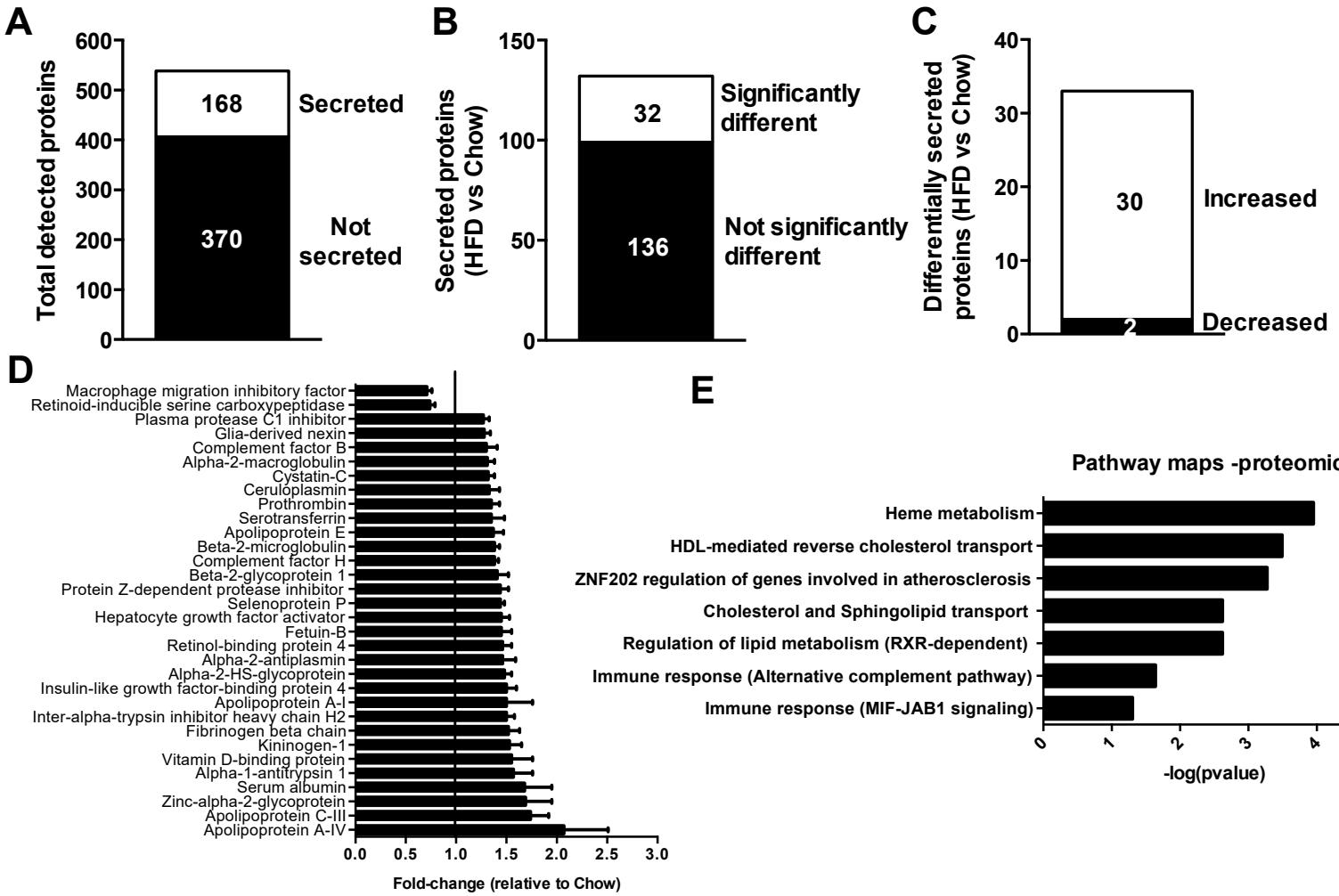
A
Total detected proteins
600
500
400
300
200
100
0
168
Secreted
370
Not secreted
B
Secreted proteins (HFD vs Chow)
150
100
50
0
32
Significantly different
136
Not significantly different
C
Differentially secreted proteins (HFD vs Chow)
40
30
20
10
0
30
Increased
2
Decreased
D
Macrophage migration inhibitory factor
Retinoid-inducible serine carboxypeptidase
Plasma protease C1 inhibitor
Glia-derived nexin
Complement factor B
Alpha-2-macroglobulin
Cystatin-C
Ceruloplasmin
Prothrombin
Serotransferrin
Apolipoprotein E
Beta-2-microglobulin
Complement factor H
Beta-2-glycoprotein 1
Protein Z-dependent protease inhibitor
Selenoprotein P
Hepatocyte growth factor activator
Fetuin-B
Retinol-binding protein 4
Alpha-2-antiplasmin
Alpha-2-HS-glycoprotein
Insulin-like growth factor-binding protein 4
Apolipoprotein A-I
Inter-alpha-trypsin inhibitor heavy chain H2
Fibrinogen beta chain
Kininogen-1
Vitamin D-binding protein
Alpha-1-antitrypsin 1
Serum albumin
Zinc-alpha-2-glycoprotein
Apolipoprotein C-III
Apolipoprotein A-IV
0.0
0.5
1.0
1.5
2.0
2.5
3.0
Fold-change (relative to Chow)
E
Pathway maps -proteomics
Heme metabolism
HDL-mediated reverse cholesterol transport
ZNF202 regulation of genes involved in atherosclerosis
Cholesterol and Sphingolipid transport
Regulation of lipid metabolism (RXR-dependent)
Immune response (Alternative complement pathway)
Immune response (MIF-JAB1 signaling)
0
1
2
3
4
5
-log(pvalue)
F
33 genes upregulated
81 genes downregulated
533 genes predicted to translate into secreted proteins
11.526 unique transcripts
15.835 probe sets detected
45.281 probe sets on the chip
G
25
7
107
CM: differentially secreted proteins
Hepatocyte transcriptome: prediction of differentially secreted proteins

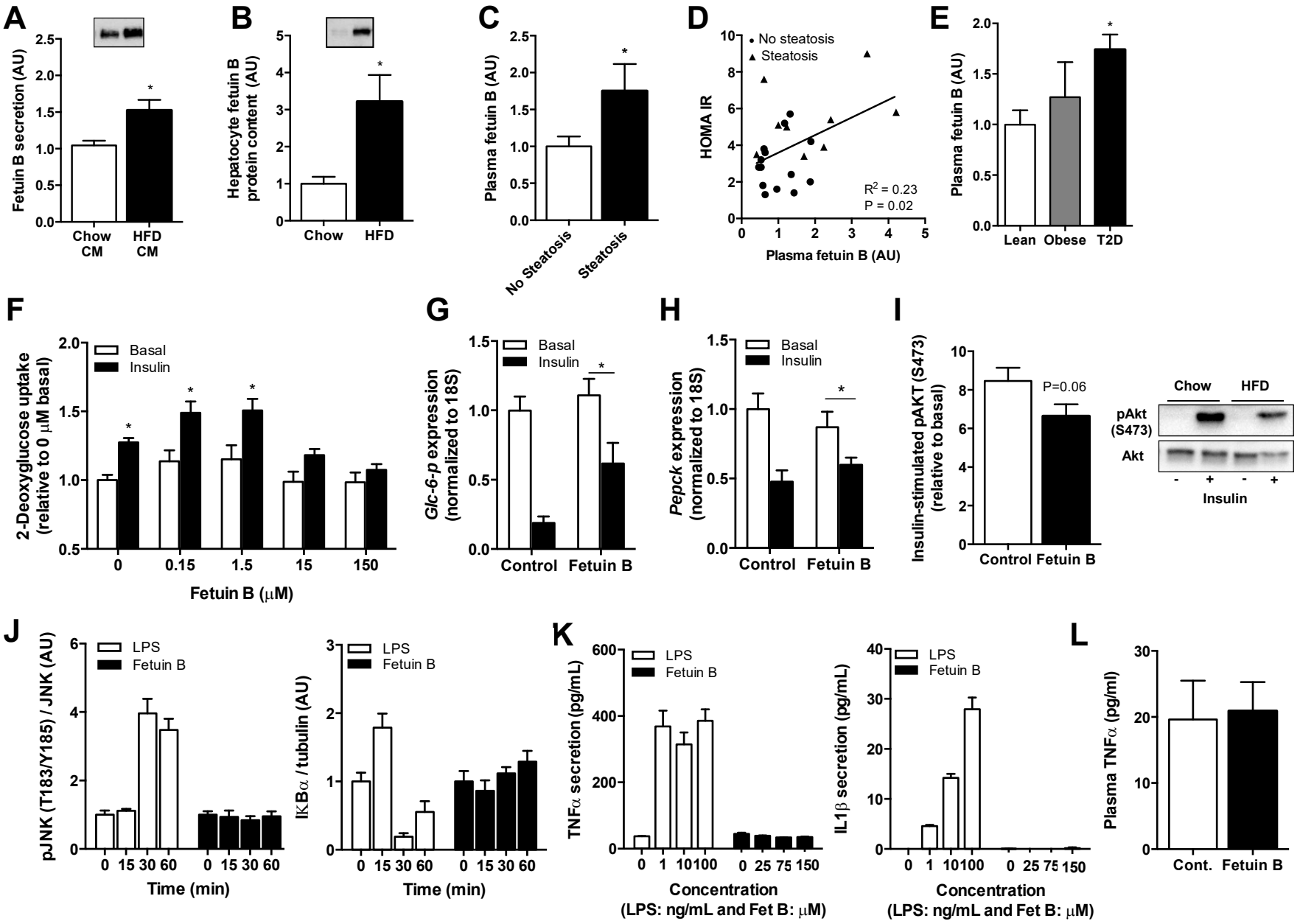
A
Fetuin B secretion (AU)
Chow CM
HFD CM
B
Hepatocyte fetuin B protein content (AU)
Chow
HFD
C
Plasma fetuin B (AU)
No Steatosis
Steatosis
D
No steatosis
Steatosis
HOMA IR
R2 = 0.23
P = 0.02
Plasma fetuin B (AU)
E
Plasma fetuin B (AU)
Lean
Obese
T2D
F
Basal
Insulin
2-Deoxyglucose uptake (relative to 0 μM basal)
Fetuin B (μM)
G
Basal
Insulin
Glc-6-p expression (normalized to 18S)
Control
Fetuin B
H
Basal
Insulin
Pepck expression (normalized to 18S)
Control
Fetuin B
I
Insulin-stimulated pAKT (S473) (relative to basal)
P=0.06
Control
Fetuin B
Chow
HFD
pAkt (S473)
Akt
Insulin
J
LPS
Fetuin B
pJNK (T183/Y185) / JNK (AU)
Time (min)
IκBα / tubulin (AU)
Time (min)
K
LPS
Fetuin B
TNFα secretion (pg/mL)
Concentration (LPS: ng/mL and Fet B: μM)
IL1β secretion (pg/mL)
Concentration (LPS: ng/mL and Fet B: μM)
L
Plasma TNFα (pg/ml)
Cont.
Fetuin B

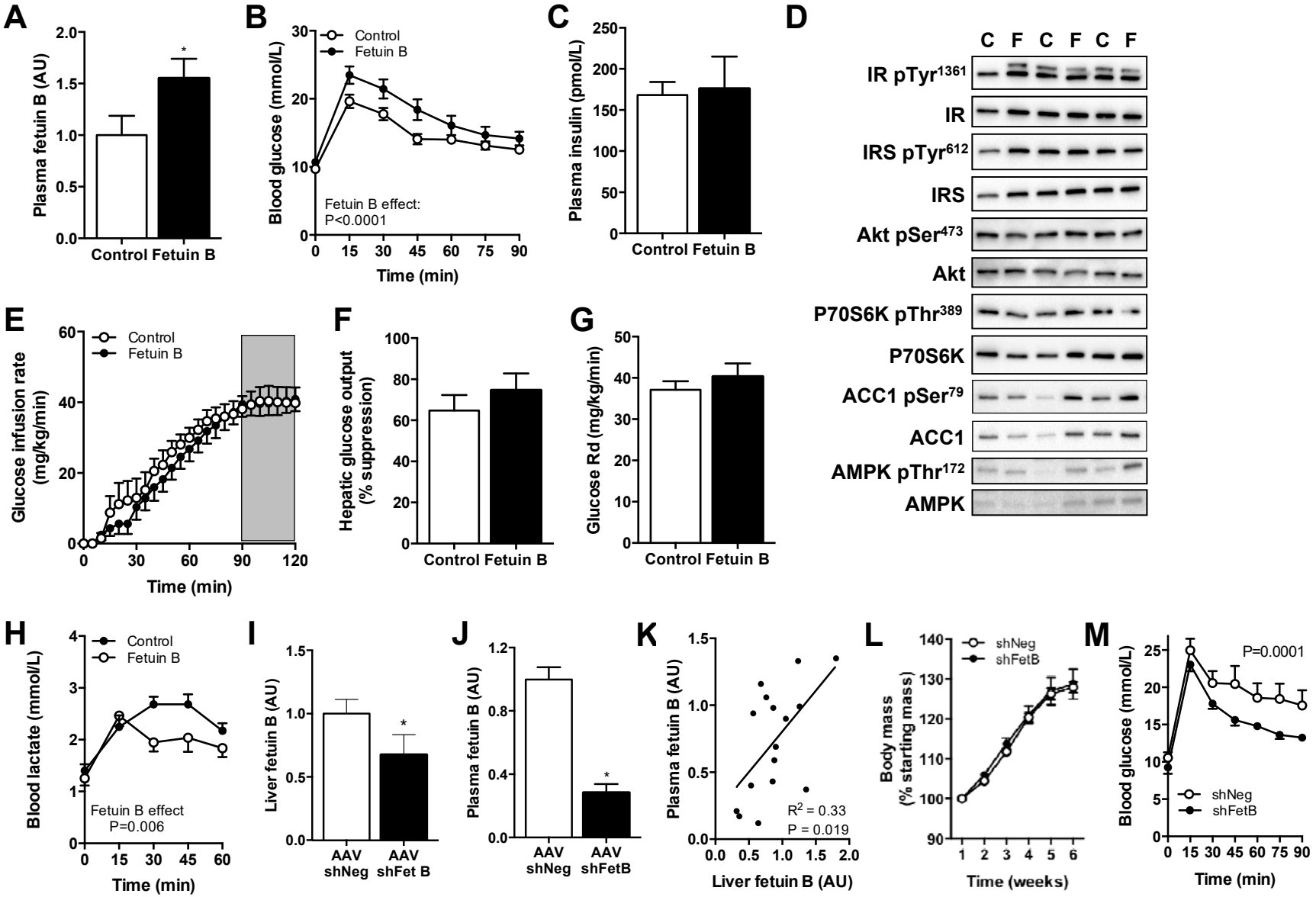
A
Plasma fetuin B (AU)
Control Fetuin B
B
Blood glucose (mmol/L)
Control
Fetuin B
Fetuin B effect:
P<0.0001
Time (min)
C
Plasma insulin (pmol/L)
Control Fetuin B
D
C F C F C F
IR pTyr1361
IR
IRS pTyr612
IRS
Akt pSer473
Akt
P70S6K pThr389
P70S6K
ACC1 pSer79
ACC1
AMPK pThr172
AMPK
E
Glucose infusion rate (mg/kg/min)
Control
Fetuin B
Time (min)
F
Hepatic glucose output (% suppression)
Control Fetuin B
G
Glucose Rd (mg/kg/min)
Control Fetuin B
H
Blood lactate (mmol/L)
Control
Fetuin B
Fetuin B effect
P=0.006
Time (min)
I
Liver fetuin B (AU)
AAV shNeg
AAV shFet B
J
Plasma fetuin B (AU)
AAV shNeg
AAV shFetB
K
Plasma fetuin B (AU)
R2 = 0.33
P = 0.019
Liver fetuin B (AU)
L
Body mass (% starting mass)
shNeg
shFetB
Time (weeks)
M
Blood glucose (mmol/L)
P=0.0001
shNeg
shFetB
Time (min)